1-1-2006

Numerical simulation of the effects of G-jitters on thermal diffusion process in binary and ternary mixtures

Chandra Adimoolam
Ryerson University

NUMERICAL SIMULATION OF THE EFFECTS OF G - JITTERS ON THERMAL DIFFUSION PROCESS IN BINARY AND TERNARY MIXTURES

by

Chandra Adimoolam, B. Tech
University of Madras, India, 2003

A thesis
presented to Ryerson University

in partial fulfillment of the
requirements for the degree of
Master of Applied Science
in the program of
Chemical Engineering

Toronto, Ontario, Canada, 2006

AUTHOR'S DECLARATION

I hereby declare that I am the sole author of this thesis.

I authorize Ryerson University to lend this thesis to other institutions or individuals for the purpose of scholarly research.

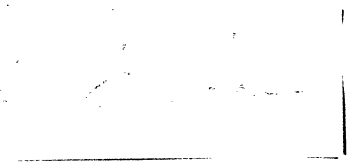

I further authorize Ryerson University to reproduce this thesis by photocopying or by other means, in total or in part, at the request of other institutions or individuals for the purpose of scholarly research.

BORROWER'S PAGE

Ryerson University requires the signatures of all persons using or photocopying this thesis. Please sign below and give the address and date.

ABSTRACT

NUMERICAL SIMULATION OF THE EFFECTS OF G - JITTERS ON THERMAL DIFFUSION PROCESS IN BINARY AND TERNARY MIXTURES

Chandra Adimoolam, Master of Applied Science, 2006,
Department of Chemical Engineering, Ryerson University

The effects of different levels of static and oscillatory gravities on the thermal diffusion phenomenon or Soret effect in binary and ternary mixtures were numerically investigated. A two dimensional square cavity is considered with lateral heating conditions. The Navier-Stokes equations, coupled with energy and mass transfer equations were solved numerically using Finite Element Method. A ternary hydrocarbon mixture consisting of methane – n-butane and dodecane and binary mixture made of water – isopropanol were analyzed to validate the applicability of the numerical method to various mixtures. The concentration, temperature and fluid flow distributions have been thoroughly analyzed for different gravity levels. The influence of gravity on the thermal diffusion process in a ternary mixture is further discussed. From the results obtained, it can be inferred that the effects of the static gravity on thermal diffusion is very significant and buoyancy convection affects the Soret separation.

ACKNOWLEDGEMENTS

I would like to extend my thanks and appreciation to my supervisors Dr. Ziad Saghir and Dr. Mehrab Mehrvar of Ryerson University, for financial support and their helpful assistance and guidance throughout the completion of this thesis. The author also acknowledges the support of Dr. Yu Yan for her assistance and useful suggestions.

I would like to acknowledge my father Adimoolam, N. and my mother Karpagam, A. for their moral support and enthusiasm for the completion of this thesis.

I would like to acknowledge the useful suggestions of my colleagues Shu Pan, Mustafa Khawaja, Baitao Jiang, Randa El-Haj, Anup Jagadeesh, Tawfiq Jaber, Amar Weli and Rakesh Patel.

I would also like to thank Ryerson University for the partial financial support.

Finally I would like to thank Natural Sciences and Engineering Council of Canada (NSERC) for their support for this project.

TABLE OF CONTENTS

LIST OF FIGURES

LIST OF TABLES

NOMENCLATURE

C_p	Specific heat at constant pressure (J/kg.K)
D_C	Mass diffusion coefficient (m^2/s)
D_T	Thermal diffusion coefficient (m^2/s. K)
g	Gravitational acceleration (m/s^2)
J_1	Mass flux of component 1 in the binary mixture (kg/m^2. s)
K	Thermal conductivity (W/m. K)
P	Pressure (Pa)
S_T	Soret Coefficient (1/K) = $\frac{\alpha_T}{T}$
t	Time (s)
u	Velocity in x-direction (m/s)
v	Velocity in y-direction (m/s)
$\overrightarrow{\nabla C}$	The vector of concentration gradient
$\overrightarrow{\nabla T}$	The vector of temperature gradient (K)

GREEK LETTERS

α_p	Pressure relaxation factor
α_T	Thermal diffusion coefficient in a binary mixture (m^2/s)
β_C	Volumetric concentration expansion coefficient
β_T	Coefficient of thermal expansion (1/K)
μ	Dynamic viscosity (kg/m.s)
ρ	Density (kg/m^3)
ψ	Volume fraction of molecules

SUBSCRIPTS AND SUPERSCRIPTS

0	Reference state
F	Firoozabadi model
H	Haase model
i	Component i
K	Kempers model
st	static component of gravity
vib	oscillatory component of gravity

CHAPTER 1

INTRODUCTION AND LITERATURE REVIEW

The thermal diffusion process, known as the Soret effect is the tendency of a convection free mixture of two or more components to separate under a temperature gradient. For binary mixtures, the Soret effect is assessed by the Soret coefficient, S_T. It is the ratio of the thermal diffusion coefficient, D_T, to the molecular diffusion coefficient D_M. However, for multi-component mixtures, the thermal diffusion coefficient is commonly used as a measure of the Soret effect. The Soret effect is an important phenomenon to study the compositional variation in hydrocarbon reservoirs. It also plays a crucial role in the hydrodynamic instability of mixtures, mineral migrations and mass transport in living matter. In reality, thermal diffusion and molecular diffusion (due to a concentration gradient) usually occur simultaneously in a fluid mixture [1]. Both diffusion processes induce mass fluxes and affect the fluid density. At the same time, the buoyancy forces may exist and drive the natural convection. This phenomenon is usually referred to as double diffusion convection.

On earth, the buoyancy convection is very strong, which makes it nearly impossible to accurately measure the thermal diffusion coefficient. The microgravity environment minimizes the effect of the gravity and allows the true diffusion limit to be achieved. Therefore nowadays performing diffusion experiments in the space appears to be a promising and feasible option [1]. However, virtually all space laboratories experience static and/or oscillatory residual accelerations called G-jitter due to the movement of the crew, aerodynamic forces, gravity gradient, solar pressure, thruster firing for altitude adjustment, operation of equipment on board, servicing activities, docking / berthing etc. G-jitters have a wide spectrum of amplitudes and frequencies. The induced convection motion, although much weaker than that on the Earth, may have a large effect on the accuracy of the thermal diffusion measurement. Theoretical modeling of the g-jitter effect, thus, becomes essential in preparing space experiments and better understanding the measurement results.

Soret effect has been studied extensively during recent years due to its importance in understanding separation related processes. This chapter gives a detailed literature review, which introduces different techniques used for measuring the Soret coefficient and also the mathematical models proposed by various researchers.

1.1 Literature Review

For years, thermal diffusion has triggered active research in both theoretical and experimental studies. Thermal diffusion in liquid phase was first observed by Ludwig in 1856 [2]. When a temperature gradient was maintained in a uniform aqueous solution of sodium sulfate it was found that a concentration gradient was established. Later, Soret discovered the effect independently and as a result thermal diffusion in the liquid phases now termed the Ludwig-Soret effect or the Soret effect.

Numerous methods have been developed to measure the Soret coefficients of binary systems with low melting points. For example, the flow cell is one technique in which the separation process occurs in a very thin flowing layer in the Poiseuille regime. The flow is separated into upper and lower halves by a sharp edge at the outlet. The difference of concentration between the two samples is analyzed by using a refractometer or densitometer. The thermo-gravitation column is a common technique, where a temperature gradient is imposed horizontally on a vertical channel. This creates a differential accumulation of different species at the top and bottom. The Soret coefficient is then evaluated from the obtained separation.

The thermal diffusion column enhances the basic separation by means of convection currents, in a manner somewhat analogous to the way a countercurrent extraction tower produces concentration differences many times those observed in a single-stage contact [3]. The thermal diffusion column consists of two opposing vertical plates separated by a narrow open space. One plate is heated and the other is cooled, and the thermal diffusion effect causes one component of, say, a binary mixture to diffuse towards the hot plate. At

the same time, the density gradient which arises because of the temperature gradient causes smooth laminar convection currents up the hot plate and down the cold. Because of the concentration gradient set up by the thermal diffusion, the convection currents transport one component preferentially toward the top and thus create large concentration differences between the top and the bottom of the column. The distance between the hot and cold plates in most thermal diffusion columns using liquids lies in the range 0.015 – 0.06 in [3].

The Soret coefficient in binary liquid mixtures can also be calculated by optical methods such as the Thermal Diffusion Forced Rayleigh Scattering (TDFRS) technique studied by Kohler *et al* [4, 6] and the Laser-Doppler Velocimetry (LDV) technique by Lepla and Wiegand [5]. The principle of TDFRS method is as follows: a grating created by the interference of two laser beams is written in a sample. A small amount of dye present in the sample converts the intensity grating into a temperature grating. This, in turn, causes a concentration grating by the effect of thermodiffusion. Both the temperature grating and the concentration grating contribute to a refractive index grating which refracts a third laser beam. The time-dependent increase and decrease in the diffracted signal intensity, after the interference grating is switched on and off, yield the diffusion coefficient D_M, the thermal diffusion coefficient D_T and the Soret coefficient S_T [5].

Perronace *et al* [7] measured the Soret coefficients and mass diffusion coefficients of n-pentane–n-decane mixture by using the Thermal Diffusion Forced Rayleigh Scattering technique (TDFRS). They used both equilibrium as well as the non-equilibrium techniques to test the ability of different molecular dynamics techniques to accurately predict the Soret coefficients. The experimental results were compared with molecular dynamics simulations values and the difference was found to be between 3% and 8% depending on the concentration.

In the Laser-Doppler Velocimetry (LDV) technique, the experimental cell consists of two horizontal copper plates that are maintained at different but constant temperatures. The

temperature difference imposed on the plates is then gradually increased in small steps. In order to allow steady state to be established, enough time is allowed between two successive temperature increments. The time dependent velocity amplitude is recorded, and, on the onset of convection, the critical temperature difference and the dimensional frequency corresponding to the oscillation of the velocity amplitude is used to calculate the Soret coefficient.

Zhang *et al* [8] developed an optical instrument to measure the Soret effect by observing the bending of a laser beam propagating horizontally through the liquid mixture subjected to a temperature gradient in the vertical direction. This technique was applied to mixtures of toluene and n-hexane over the temperature range 5 – 45°C and to mixtures of ethanol and water at 25°C. The accuracy of the technique was increased by substantially reducing the transient time for applying a temperature gradient and by improving the horizontal temperature uniformity along the liquid layer, combined with an increase of the path length of the optical beam in the liquid layer. The design of the liquid cell, with a long path length and controlled temperature uniformity, enabled the researchers to measure Soret coefficients with an accuracy of 1–3%, higher than that obtained by previous investigators.

The thermal diffusion in packed columns (TPC) refers to an instance when diffusion takes place due to thermal gradient when a porous medium is present in the column. Filling the tubular space with a porous medium reduces the rate of the convection because the fluid moves slowly in porous media and allows large separations [3]. The porous medium also regulates the velocity of the fluid for obtaining optimal coupling between the two physical processes i.e. buoyancy and thermal diffusion, which leads to thermogravitational diffusion [9]. The mass separation in a thermogravitational column depends on the balance between two rates— (i) the rate of mass flux (due to the basic thermal diffusion effect) in the horizontal direction and (ii) the convection velocity in the vertical direction. Hence, anything that decreases the convection velocity, such as introducing packing material, increases the relative importance of the horizontal flux, and

thus increases the steady state mass separation in the batch column [9]. A study by Lorenz and Emery [3] shows that the maximum magnitude of separation or the optimum coupling between buoyancy and thermal diffusion is obtained at a particular value of the permeability. They also found that the packed column offers the advantage of using columns constructed with fewer intricacies.

Costeseque *et al* [10] conducted experiments to measure the Soret coefficient of a binary mixture consisting of water – alcohol with a 10% mass fraction of ethanol or propanol. The two methods that were used by the researchers are (i) flat-packed Soret cell operated under a vertical thermal gradient and (ii) the packed cylindrical thermodiffusion column operated with a horizontal thermal gradient. The porous packing was made of inert balls (ZrO_2) with a porosity of 38%. They observed that the performance of the evaluation method for the Soret coefficient depends on the type of cell used. In the packed thermogravitational column, the values were obtained from modeling a 0.5% error in experimental values. Whereas the Soret coefficient was directly measured from the experimental values in the packed Soret cell and an average value obtained. They also concluded that the packed Soret cell had a great advantage because the experimental period was only 7 days whereas the packed thermogravitational column method took 60 days. Considering the duration of the experiments, alcohol was better preserved with less evaporation in Soret cell, which means less deviation in the experimental data.

Several researchers have published the Soret coefficient values for organic molecules, polymers and electrolyte solutions. However, few data are available from various techniques on the same systems. In summer 1999, research groups from various universities started a ground-based measurement campaign to establish a reliable database of the Soret coefficient for binary mixtures. They investigated three binary mixtures of Dodecane ($C_{12}H_{26}$), Isobutyl benzene (IBB) and 1,2,3,4 Tetrahydronaphthalene (THN) at a mean temperature of 25^0 C which contained a mass fraction of 0.5 of each component [11]. The different techniques that were used by the researchers to measure the Soret coefficients are TDFRS, annular thermogravitational

column and LDV. The values obtained from independent researchers, were in strong agreement with each other [11], their differences did not exceed more than 7%. The Soret coefficient for three binary mixtures of (i) THN - Dodecane, (ii) THN - IBB and (iii) IBB – Dodecane, all with a mass fraction of 50% for each component were found to be $(9.5 \pm 0.5) \times 10^{-3}$ K^{-1}, $(3.3 \pm 0.3) \times 10^{-3}$ K^{-1} and $(3.9 \pm 0.1) \times 10^{-3}$ K^{-1}, respectively at the mean temperature of 25°C.

Within the framework of the international benchmark test, Costeseque and Loubet [12] measured the porous medium thermodiffusion coefficient D_T^* of two hydrocarbon binary mixtures: THN – dodecane and THN – IBB where the weight fraction of each component was near 50 wt%. The porous medium thermodiffusion coefficient D_T^* of the mixtures (i) THN – dodecane and (ii) THN – IBB were found to be $(3.04 \pm 0.25) \times 10^{-12}$ m^2 s^{-1} K^{-1} and $(1.44 \pm 0.15) \times 10^{-12}$ m^2 s^{-1} $K^{-}1$ respectively.

Dutrieux et al [13] reported Soret coefficients obtained by two independent methods and for two different binary systems. The binary systems were made of water-ethanol containing 60.88 and 50 wt% of water, respectively. In the first method, thermal diffusion coefficient was determined by a thermo-gravitational column and molecular diffusion coefficient by the well-known open-ended capillary technique (OEC) [13]. In the other method the LDV technique was used to measure the velocity of a transient natural convective state: indeed, the Soret effect induces modifications of density gradients and therefore the buoyancy responsible for free or natural convection. The Soret coefficient was determined indirectly by the modifications of the convective amplitudes.

Kohler et al [4] reported the Soret coefficients and mass diffusion coefficients of mixtures of toluene and n-hexane measured by using the TDFRS technique. The experiments were performed on the mixtures with toluene mole fractions of 0.25, 0.5, and 0.75 at 23°C. The sample with a mole fraction of 0.5 was also performed at 30°C and 38 °C to allow a direct comparison with the data reported by Ecenarro *et al* [4]. Since no agreement was found with the literature data for toluene-n-hexane mixtures, the researchers made an additional measurement for ethanol-water mixture with an ethanol

weight fraction of 0.391 at a temperature of 25°C. The diffusion coefficient of the ethanol-water mixture was obtained to be $D_M = 4.19 \times 10^{-6}$ cm^2 s^{-1} and the Soret coefficient to be $S_T = -3.25 \times 10^{-3}$ K^{-1}, which was in excellent agreement with the values reported by Kolodner *et al.* [4] who found $D_M = 4.19 \times 10^{-6}$ cm^2 s^{-1} and $S_T = -3.16 \times 10^{-3}$ K^{-1}.

A new model was presented for the prediction of thermal diffusion coefficients in binary mixtures of reservoir fluids using the thermodynamics of irreversible processes by Shukla and Firoozabadi [14]. Equilibrium properties, such as partial internal energies and fugacities needed for the model were obtained from the volume translated Peng-Robinson equation of state, while viscosity was accounted for by incorporating the energy of viscous flow. The model was applied to predict thermal diffusion coefficients of several mixtures consisting of both non-hydrocarbon and hydrocarbon fluids. Theoretical results of the model were validated with the experimental data obtained for the binary systems namely C_1/C_3, C_1/C_4, C_7/C_{12}, C_7/C_{16}. In general, the Firoozabadi model is superior in describing the experimental results for the thermal diffusion coefficients in binary mixtures by the comparisons between theoretical and experimental data. In particular, the sign of thermal diffusion coefficient is consistent with the experimental data.

Simon *et al* [15] employed the Direct Non-Equilibrium Molecular Dynamics (NEMD) simulations to compute the thermal conductivity and the thermal diffusion coefficient in a methane-n-decane binary mixture in the liquid state. This study also emphasizes the fact that using direct-NEMD, there is no need for additional calculation of any thermodynamic property of the mixture. The thermal conduction data computed from direct NEMD when compared with previous experimental results were in excellent agreement, and the general behaviour with temperature and density was consistent with experimental results on binary mixtures in the liquid state. They checked the validity of the method by comparing the simulated data with the values predicted by Assael *et al* [15] and the difference between the simulated and predicted data was found not to exceed 6%.

There have been extensive experimental and theoretical studies of thermal diffusion coefficients in binary mixtures. However, there is little data available on the measurement of thermal diffusion coefficients in ternary, non-electrolytes and higher mixtures. This is due to the fact that there is more complexity in the diffusion coefficients (thermal, molecular, and pressure) of ternary mixtures in comparison to those of binary mixtures. Furthermore, the appearance of cross-molecular diffusion complicates the coefficients in ternary and higher mixtures [16].

Kita *et al.* [17] measured the polymer Soret coefficient of polyethylene oxide (PEO) in a water-ethanol solvent ternary mixture. It was based on the assumptions of (i) a negligible cross-molecular diffusion and (ii) a fluid phase ideality, in the sense that there is no volume change on mixing. They investigated the temperature dependence of the Soret coefficient for water-rich polymer solutions and the results revealed a sign change from negative to positive as the temperature is increased and the sign change took place at a water mass fraction of 0.83 at a temperature of 22°C. On the other hand, for low water content, the Soret coefficient of the polymer was found to be negative, i.e., the polymer migrated to the warmer regions of the fluid. They concluded that specific interactions (hydrogen bonds) between solvent molecules and between polymer and solvent molecules play an important role in thermodiffusion for this system.

Leahy-Dios *et al.* [16] measured the thermal diffusion coefficients in three ternary mixtures. The ternary mixture composition consisted of (i) Dodecane (33.3%), THN (33.3%), IBB (33.4%), (ii) octane (33.3%), decane (33.3%), 1-methylnaphthalene (33.3 %) (iii) Octane (16.7%) – decane (16.7%) -1-methylnaphthalene (66.6%) all mass percent. The results of ternary mixtures of octane-decane-1-methylnaphthalene showed a sign change of the thermal diffusion coefficient for decane as the composition changes, despite the fact that the two normal alkanes were similar. They also measured the binary thermal diffusion factors which consisted of octane, decane and 1-methylnaphthalene. The results revealed a remarkable difference in the thermal diffusion behavior in binary and ternary mixtures

Given the fact that the transport coefficient data for binary and ternary mixtures are sparsely available, it is already known that the variation of hydrocarbon reservoirs—a non-ideal multi-component mixture system—cannot be determined using results obtained from binary or ternary mixtures since diffusion coefficients may significantly differ in multi-component mixtures. Furthermore, the direction of the component segregation in the hot or cold regions for multi-component mixture systems is not defined on the sign of the thermal diffusion factors. The formalism is more complicated for non-ideal multi-component mixtures, and the interaction theory of all chemical species present in the mixture is still not fully developed. Further work is being carried out presently to understand the species behaviour in systems far from concentration equilibrium and to determine the diffusion process in multi-component mixtures.

Kempers [18] presented a comprehensive theory for the Soret effect which incorporates both the thermodynamic contribution from selective attraction / repulsion and the kinetic contribution from selective collision interaction between the components. This theory yields a set of working equations for calculating thermal diffusion factors for multi component mixtures as well as binary mixtures. This is an extension of the theory he presented earlier [18] where the thermodynamic contribution only was modeled. He compared the results obtained from his theory with the data available form the literature. Since the calculation of the Soret effect is extremely sensitive to the accuracy of input from the equation-of-state, closer agreement was not obtained. He concluded that due to the higher demand in accuracy, even the present equations-of-state that are calibrated for use in the chemical and petroleum industry, required modification for the calculation of the Soret effect.

Haughen and Firoozabadi [19] investigated the steady-state separation of the individual components of an incompressible multicomponent liquid mixture. This theory is based on the main assumptions that (i) the effect of composition variation on density and (ii) the effect of vertical molecular diffusion are negligible. They derived the analytic working equations for measuring thermal diffusion coefficients which are analogous to the

existing equations for a binary mixture. They found that compositional variation had negligible effect on fluid density and molecular diffusion does not affect steady-state separation which is similar to the binary mixture results.

It is common that thermal diffusion and molecular diffusion having different diffusivities occur simultaneously in a fluid mixture. The buoyancy forces drive the natural convection and make the fluid flow more complicated. This phenomenon is usually referred to as double diffusion convection. Under territorial conditions, the buoyancy convection is very strong, which makes it difficult to accurately measure the thermal diffusion coefficient. One possible remedy to overcome this problem is to minimize the buoyancy by performing experiments in microgravity on free flying platforms, such as the International Space Station (ISS) and FOTON. Without the buoyancy-induced convection, experiments under such conditions may lead to accurate measurement of the thermal diffusion coefficient. In order to better understand the influence of these variations during microgravity experiment, Chacha *et al.* [1] simulated the double diffusion process under several thermal boundary conditions. These included smooth change in the lateral thermal boundary condition, radiating horizontal walls, and even more drastic, the abrupt change in the lateral thermal boundary condition. It was observed that when there is a strong convection, secondary recirculation eddies form along the corners of the cavity and a clockwise rotating cell is present in the center of the cavity. This cell formation indicates the strength of convection inside the cavity. The temperature profile near the hot and cold walls was distorted due to the presence of convection. As well, the heat transfer due to convection is stronger and faster than the heat transfer due to conduction. Therefore, they concluded that the transport of heat is driven by the convective flow in the boundary layers, as well as in normal gravity. In the case of radiating horizontal walls, it was observed that a stronger radiative heat loss, or, a high emissive or a very weak temperature difference between the end walls, could possibly lead to the break up of the entire cavity into different thermodiffusion sub-cells. This would hence result in greater uncertainties in the Soret coefficient measurements. Further, it was observed, in the event of power outage during an experiment in space that the system responds with some delay to the modification of the boundary conditions.

Conducting experiments in microgravity environments in space since the absence of the buoyancy convection may maximize the accuracy of the measurement. However, virtually all Space laboratories experience steady and/or oscillatory residual accelerations called microvibration or g-jitter. This g-jitter may be due to the movement of the crew, aerodynamic forces, gravity gradient, solar pressure, thruster firing for altitude adjustment, operation of equipments on board, servicing activities, docking / berthing etc. The existence of g-jitter does induce a convection motion which in turn affects the diffusion dominated experiments. The degree that the g-jitter will affect the accuracy of the measurement depends on its magnitude and alignment. It is therefore important to analyze the effect of g-jitters on diffusion processes for better interpretation of the experimental results from the Space laboratories.

Gershuni *et al* [20] studied the problem of convection and convective instability of a fluid in a high frequency vibration field under low gravity conditions. They discussed the equilibrium conditions and also determined the boundary of vibrations for some equilibrium states — (i) a plane layer of fluid with transverse temperature gradient and arbitrary direction of vibration, (ii) a cylindrical layer with radial gradient and longitudinal direction of vibration, and (iii) an infinite circular cylinder with transverse and mutually perpendicular directions of the temperature gradient and the vibration axis. The onset of convection occurs when the Rayleigh number reaches some critical value. They determined the critical values of Rayleigh number and the characteristics of the critical disturbances. They concluded that for a binary mixture in an infinite horizontal layer in the presence of vertical high frequency vibration, the effect of vibration was purely stabilizing. And also with increasing vibrational parameter the critical Rayleigh number increased monotonously.

A numerical study was carried out by Savino [21] for the evaluation of the thermo-fluid-dynamic disturbances induced by residual-g and g-jitter on the International Space Station (ISS) for two classes of experiments that exhibit a large sensitivity to accelerations — (i) measurement of the thermal conductivity in high Prandtl number liquids and (ii) measurement of the thermodiffusion coefficient in binary mixtures. He

performed numerical simulations to compare the results obtained by the direct integration of the full Navier-Stokes equations with the solutions of the equations for the time-averaged quantities (thermovibrational theory). The results showed that, for the microgravity environment of the ISS, the two formulations gave almost the same results. From the simulations at different orientations of the residual-g and g-jitter he concluded that, orienting the residual-g parallel to the density gradient reduces the convective disturbances and can also help mitigating the disturbances induced by the g-jitter.

Chacha *et al* [22] investigated the role of thermal diffusion phenomena on compositional variation in a binary mixture of methane and n-butane in the presence of a fluctuating acceleration field. The mixture was contained in a rectangular cavity subject to heat losses on its horizontal walls and a temperature difference between its vertical walls. They considered the amplitude of the oscillatory gravity (g-jitter) to be greater than the static gravity (residual gravity). The researchers concluded that the presence of the g-jitter in the vertical or horizontal direction led to the progressive remixing and therefore butane distribution became uniform with increasing time. In the case of a fluctuating gravity field parallel to the main density gradient remixing was found to be stronger. Buoyancy and mass-thermo-vibrational effects were completely eliminated by orienting the facility in such a way that the density gradient and the acceleration directions were aligned. They also indicated that when the g-jitter and the residual gravity act in the vertical direction (orthogonal to the main density gradient), the velocities were larger and the distortions of the isotherms from the purely diffusive situation reached the maximum.

Savino *et al* [23] investigated the effects of disturbances on a typical microgravity experiment for the measurement of the diffusion coefficients in liquids. They developed a mathematical model for the general case of a binary mixture which included both buoyancy and vibrational driving actions with simultaneous temperature and concentration gradients. After analyzing the numerical results they concluded that residual-g of the order of magnitude of $g_0 \approx 10^{-6}$ was responsible for a negligible error in the measurement of the diffusion coefficient, whereas more relevant distortion was associated with extremely large g-jitters.

Monti *et al* [24] reported a series of theoretical work on the effects of g-jitter disturbances for the measurement of the diffusion coefficients in liquids on the ISS platform. They investigated the transient effects induced by g-pulses and g-jitters of finite duration by numerical solutions, using the direct formulation and a time-averaged formulation. They found out that for a temperature gradient orthogonal to the gravity vector, the second pulse somehow compensates the first one. On the contrary in the case of a temperature gradient parallel to the gravity vector the second pulse may be stabilizing or destabilizing, depending on the orientation of the gravity vector.

Yan *et al* [32] investigated the double diffusive convection of water – alcohol mixtures in a cubic cavity. They demonstrated a three-dimensional numerical model for the binary mixture of water-isopropanol (90:10 wt %) subject to the lateral heating condition and at various gravity levels. They also discussed the influence of gravity induced convection on the thermal diffusion process. From the analysis they found that the static gravities with large magnitude have the most hazardous effect on the diffusion process. When compared to the static gravities, the oscillatory gravities with large amplitude also have negative, although smaller effect. The study reveals the importance of removing both gravities in the fluid science experiments in Space in order to achieve near zero gravity condition to ensure the accuracy of the experiments.

Research Objective

The main objective of this research is to study numerically the effects of vibration on the thermal diffusion process carried out on the International Space Station in binary and ternary hydrocarbon mixtures. Vibrations are caused due to the movement of crew, thruster firing etc. The hydrocarbon mixtures consist of methane – n-butane and dodecane.

CHAPTER 2

FUNDAMENTAL THEORY OF THERMAL DIFFUSION

2.1 Theoretical Models of Thermal Diffusion

Although the thermal diffusion coefficient can be measured through different techniques, to avoid the possible occurring effect of thermal convection, the measurement condition has to be strictly controlled which is very difficult in ground conditions. Over years of extensive studies about this phenomenon researchers have come up with reliable thermal diffusion coefficient models. Several theoretical approaches have been proposed for binary mixtures with various degrees of success. The phenomenological theory of irreversible thermodynamics by Haase [26], the kinetic theory of irreversible thermodynamics by Rutherford [27], Dougherty and Drickamer [28] and Shukla and Firoozabadi [14] and the maximization of the partition function of two idealized bulbs by Kempers [29] are to name a few. In all of the above mentioned models, partial molar properties are required which are derived from the equation of state (EOS). Hence, for any particular mixture, the accuracy of the model not only relies on the model itself, but also on both the EOS of choice and the numerical method utilized in the calculation. Below, three models are listed and described briefly.

2.1.1 Haase Model

The Haase [23] model is based on the phenomenological approach which uses the phenomenological equations of irreversible thermodynamics to derive the following equations for binary systems in terms of the net heat transport and chemical potential:

$$\alpha_T = \frac{Q_2^* - Q_1^*}{x_1(\partial\mu_1/\partial x_1)} \tag{2.1}$$

where α_T is the thermal diffusion factor in a binary mixture, x_1 is the mole fraction of component 1, μ_1 is the chemical potential of component 1, and Q_i^* is the net heat transport of component i (i = 1, 2).

The chemical potential or the partial molar Gibbs free energy is given by

$$\mu i = \left.\frac{\partial G}{\partial n_i}\right|_{T,P,n_{j\neq i}} dn_i \tag{2.2}$$

The thermal diffusion factor is usually applied in experimental analysis and can be obtained based on measured data. The Soret coefficient is given by

$$S_T = \frac{\alpha_T}{T} \tag{2.3}$$

where the T is absolute temperature.

the Soret coefficient S_T is defined by

$$S_T = \frac{D_c}{D_T}$$

Assuming that in a mass conserved system, the net heat of transport is interpolated with the molar enthalpy, and with the thermostatic values of enthalpy the net heat of transport is expressed as:

$$Q_2^* - Q_1^* = \frac{M_1 M_2}{M_1 x_1 + M_2 x_2}\left(\frac{H_2}{M_2} - \frac{H_1}{M_1}\right) \tag{2.4}$$

where H_i is the partial molar enthalpy of component i (i =1, 2) and M_i is the molecular weight of component i (i =1, 2). The thermal diffusion factor in the Haase model can be expressed as

$$\alpha_T^H = \frac{M_1H_2 - M_2H_1}{(M_1x_1 + M_2x_2)x_1(\partial\mu_1/\partial x_1)} \tag{2.5}$$

For ideal gas or liquid at a reference temperature, equation (5) gives

$$\alpha_T^0 = \frac{M_1H_2^0 - M_2H_1^0}{(M_1x_1 + M_2x_2)RT} \tag{2.6}$$

where R is the gas constant. Then, the Haase model, with regard to a reference state may be re-written as:

$$\alpha_T^H = \frac{\alpha_T^0 RT(M_1x_1 + M_2x_2) + M_1(H_2 - H_2^0) - M_2(H_1 - H_1^0)}{(M_1x_1 + M_2x_2)x_1(\partial\mu_1/\partial x_1)} \tag{2.7}$$

2.1.2 Kempers Model

The Kempers [31] model is based on a statistical description of a non-equilibrium two-bulb system, assuming that a system with a fixed volume at a uniform pressure without external forces. The expression for net heat transport is given by

$$Q_2^* - Q_1^* = \frac{V_1V_2}{V_1x_1 + V_2x_2}\left(\frac{H_2}{V_2} - \frac{H_1}{V_1}\right) \tag{2.8}$$

where V_i is the partial molar volume of component i, and H_i is the partial molar enthalpy of component i (i =1, 2).

Combining equations (2.1) and (2.6), the thermal diffusion factor in the Kempers model is given by:

$$\alpha_T^K = \frac{V_1 H_2 - V_2 H_1}{(V_1 x_1 + V_2 x_2) x_1 (\partial \mu_1 / \partial x_1)} \tag{2.9}$$

2.1.3 Shukla — Firoozabadi Model

Firoozabadi et al. [10, 15] presented a model for binary mixtures of reservoir fluids, based on the irreversible thermodynamics of processes. In this model, the net heat of transport is related to the energy of detaching a molecule from its neighbours in the region of the mixture, and to the energy given up in that region when one molecule fills a hole. This energy is expressed in terms of the partial molar internal energy and the ratio of the energy of vaporization to the energy of viscous flow of the component. The net heat of transport is given by

$$\begin{cases} Q_1^* = W_{H1} - \psi_1 (x_1 W_{H1} + x_2 W_{H2}) \\ Q_2^* = W_{H2} - \psi_2 (x_1 W_{H1} + x_2 W_{H2}) \end{cases} \tag{2.10}$$

where ψ_i gives the volume fraction of molecules moving into a hole left by a molecule of type i in the mixture. This can be expressed in terms of molar fractions x_i (i =1,2) and partial molar volumes V_i (i =1,2) as follows:

$$\begin{aligned} \psi_1 &= V_1 / (x_1 V_1 + x_2 V_2) \\ \psi_2 &= V_2 / (x_1 V_1 + x_2 V_2) \end{aligned} \tag{2.11}$$

subject to the constraint of the Gibbs-Duhem relation

$$x_1 \psi_1 + x_2 \psi_2 = 1 \tag{2.12}$$

and

$$\begin{cases} W_{H1} = -U_1 / \tau_1 \\ W_{H2} = -U_2 / \tau_2 \end{cases} \tag{2.13}$$

where U_i is the partial molar internal energy of component i (i =1, 2), and τ_i is the ratio of the energy of vaporization, ΔU^{vap}, and the energy of viscous flow, ΔU^{visc}, i.e.,.

$$\tau_i = \Delta U_i^{vap} / \Delta U_i^{visc} \tag{2.14}$$

Substituting equation (2.10) to (2.14) into equation (2.1), the thermal diffusion factor is thus given by:

$$\alpha_T^F = \frac{\left(U_1 / \tau_1 - U_2 / \tau_2\right)}{x_1 \left(\partial \mu_1 / \partial x_1\right)} + \frac{\left(V_2 - V_1\right)\left(x_1 U_1 / \tau_1 + x_2 U_2 / \tau_2\right)}{\left(V_1 x_1 + V_2 x_2\right) x_1 \left(\partial \mu_1 / \partial x_1\right)} \tag{2.15}$$

In this model, the thermal diffusion factor is an explicit function of partial molar internal energy, partial molar volumes, the chemical potential and the ratio of the energies of vaporization and viscous flow. The value of ratio, τ_i, is estimated to be 4.0 for most of the non-associated liquids and hydrocarbons.

2.2 Governing Equations

The basic laws of science and engineering are expressed by the partial differential equations. PDE's provide the foundation for modeling a wide range of scientific and engineering phenomena. The basic governing equations for a dynamic two dimensional model are given below.

2.2.1 Momentum Conservation Equation

The principle of momentum conservation is represented by the Navier–Stokes equations. For a two dimensional case, the momentum equation in the x direction is given by

$$\frac{\partial}{\partial t}(\rho u)+\frac{\partial}{\partial x}(\rho uu)+\frac{\partial}{\partial y}(\rho uv)=-\frac{\partial p}{\partial x}+\mu\left(\frac{\partial^2 u}{\partial x^2}+\frac{\partial^2 u}{\partial y^2}\right) \tag{2.16}$$

where ρ is the fluid density, u and v are the velocity components in the x and y directions respectively and t denotes the time.

In the y direction it is given by

$$\frac{\partial}{\partial t}(\rho v)+\frac{\partial}{\partial x}(\rho uv)+\frac{\partial}{\partial y}(\rho vv)=-\frac{\partial p}{\partial y}+\mu\left(\frac{\partial^2 v}{\partial x^2}+\frac{\partial^2 v}{\partial y^2}\right)+f_y \tag{2.17}$$

where f_y is the body force term given by

$$f_y=-\rho g\left[1-\beta_T(T-T_m)+\beta_c(C-C_0)\right] \tag{2.18}$$

The pressure is denoted by p, and μ is the dynamic viscosity of the mixture. β_T and β_c are the thermal and concentration expansion coefficients respectively. The average temperature and solute mass fraction in the cavity are denoted by T_m and c_0 respectively.

2.2.2 Mass Conservation Equation

The conservation of mass can be expressed by the partial differential continuity equation as follows:

$$\frac{\partial \rho}{\partial t}+\frac{\partial \rho u}{\partial x}+\frac{\partial \rho v}{\partial y}=0 \tag{2.19}$$

Since the fluid is composed of two non-reacting species, the principle of mass conservation applies to each individual component as well as to the mixture as a whole. For each component and in terms of the mass fraction c, the principle of mass conservation results in an equation of the form

$$\rho\left(\frac{\partial C}{\partial t}+u\frac{\partial C}{\partial x}+v\frac{\partial C}{\partial y}\right)=-\vec{\nabla}\bullet\vec{j} \tag{2.20}$$

where $\vec{j}$ is the total flux which is given by

$$\vec{j}=-\rho\left[D_c\vec{\nabla}C+D_T\vec{\nabla}T\right] \tag{2.21}$$

the total flux $\vec{j}$ comprises of a Fickian diffusive flux (first term) and a thermal diffusive flux (second term). Eq. (2.20) is used for the solute conservation within the cavity, the concentration of the second component (carrier-fluid) is equal to 1 – C. The terms Dc and D_T represent the mass diffusion and the thermal diffusion coefficients, respectively, which are assumed to be constant in our analysis. The expanded form of the equation is

$$\frac{\partial C_i}{\partial t}+u\frac{\partial C_i}{\partial x}+v\frac{\partial C_i}{\partial y}=\left(D_c\frac{\partial^2 C_i}{\partial x^2}+D_T\frac{\partial^2 T}{\partial x^2}\right)+\left(D_c\frac{\partial^2 C_i}{\partial y^2}+D_T\frac{\partial^2 T}{\partial y^2}\right) \tag{2.22}$$

where C_i is the concentration of component i.

2.2.3 Energy Conservation Equation

Assuming that there is no internal heat generation, the principle of conservation of energy is expressed by the following equation:

$$\rho\left(\frac{\partial T}{\partial t}+u\frac{\partial T}{\partial x}+v\frac{\partial T}{\partial y}\right)=\frac{k}{C_p}\left(\frac{\partial^2 T}{\partial x^2}+\frac{\partial^2 T}{\partial y^2}\right) \tag{2.23}$$

where C_p and k are the specific heat and the thermal conductivity respectively of the fluid, assumed to be constant, and T is the temperature.

2.2.4 Boussinesq Approximation

It assumes that the density variations matter only in the body force term, not in the inertial terms. It reduces the nonlinearity and applicable for slowly varying flows.The Boussinesq approximation is used for bouyancy driven flows. The basis of this approximation is that the density variations are sufficiently small to be neglected, except where they appear in terms multiplied by g, the acceleration due to gravity. Boussinesq flows are common in industries such as dense gas dispersion, fume cupboard ventilation to name a few. The approximation is extremely accurate for many such flows, and makes the mathematics and physics simpler since it reduces the nonlinearity in the governing equations.

For example, when the fluid density changes only with temperature, the density can be represented as:

$$\rho_f = \rho_0[1 - \beta_T(T - T_0)] \tag{2.24}$$

where, ρ_0 is the fluid density, the subscript 0 refers to a reference state and β_T is the coefficient of thermal expansion due to the temperature change.

When there are small isobaric changes in the temperature and concentration, the mixture density ρ depends linearly on both T and C, which is the case of double-diffusive convection.

$$\rho = \rho_0[1 - \beta_T(T - T_0) - \beta_C(C - C_0)] \tag{2.25}$$

The coefficient of thermal expansion β_T is given as,

$$\beta_T = -(1/\rho)(\partial\rho/\partial T)_{p,C} \tag{2.26}$$

The volumetric concentration expansion coefficient β_C is given by:

$$\beta_C = -(1/\rho)(\partial\rho/\partial C)_{T,p} \tag{2.27}$$

2.3 Numerical Solution

The conservation equations are used to calculate flow patterns or variations in complex geometries. For such problems, it is generally not possible to calculate an analytical solution of the governing equations. We use numerical methods such as **Finite Volume** or **Finite Element Methods** to solve this kind of problems. In solving fluid flow problems one should be aware that the underlying physics is complex and the results generated by a CFD code are at best as good as the physics embedded in it. A good understanding of the numerical algorithm is also crucial to obtain a reliable solution.

Three mathematical criteria are useful in determining the success of such algorithms: convergence, consistency and stability. **Convergence** is the property of a numerical method to produce a solution which approaches the exact solution as the grid spacing, control volume size or element size is reduced to zero. **Consistent** numerical schemes produce systems of algebraic equations which can be demonstrated to be equivalent to the original governing equation as the grid spacing tends to zero. **Stability** is associated with damping of errors as the numerical method proceeds. If a technique is not stable even roundoff errors in the initial data can cause divergence [30].

2.3.1 Finite Element Method (FEM)

Finite Element Method is a numerical method for solving problems of engineering and mathematical physics. Typical problems include: Structural analysis, heat transfer, Fluid flow, Mass transfer, Electro-Magnetic potential etc. The governing equations of such systems are generally in the form of ODE's or PDE's. It is always not possible to obtain

the analytical solutions to these systems due to the complicated geometries. Hence we need to rely on numerical methods such as Finite Element Methods.
The domain of interest is divided into an assembly of finite elements which are connected by nodes. FEM reduces the PDE's to a system of algebraic equations for solution. This method yields approximate values of the unknowns at discreet number of points in a continuum. Generally, PDE will contain a function $u(x)$ defined for all x in the domain, with respect to some given boundary conditions. The finite element method is used to determine an approximation to the function $u(x)$. The method requires the discretisation of the domain into sub-regions or elements. On each element, the function is approximated by a characteristic form, and $u(x)$ can be approximated by a linear function.

To summarize in general terms how the finite element method works, the main steps are listed [31]:

1. Domain discretization: The first step in FEM is to divide the solution region into finite elements. The description of mesh consists of several arrays main of which are nodal coordinates and element connectivities. In this study the Central Difference scheme was used for domain discretization.

2. Selection of shape functions: Interpolation functions are used to interpolate the field variables over the element. Often, polynomials are selected as interpolation functions. The degree of the polynomial depends on the number of nodes assigned to the element. 2^{nd} order Lagrange elements were used as interpolation functions.

3. Developing the element equations: The matrix equation for the finite element is established which relates the nodal values of the unknown function to other parameters. For this task different approaches can be used; the most convenient is the Galerkin's method.

4. Assembling the element equations: To find the global equation system for the whole solution region we must assemble all the element equations. In other words we must combine local element equations for all elements used for discretization. Element connectivity is used for the assembly process. Before solution, boundary conditions (which are not accounted in element equations) should be imposed.

5. Solving the global equation system: The finite element global equation system is typically sparse, symmetric and positive definite. Direct and iterative methods can be used for solution. The nodal values of the sought function are produced as a result of the solution.

6. Computing additional results: In many cases we need to calculate additional parameters. For example velocity contours, temperature distribution etc.

2.4 Numerical Solution Technique

FEMLAB is a powerful interactive software for modeling and solving scientific and engineering problems based on Partial Differential Equations. Using this software we can couple and solve multiphysics models. FEMLAB uses Finite Element analysis together with adaptive meshing and error control using a variety of numerical solvers. FEMLAB can be used in many application areas like Chemical Reactions, Heat Transfer, Fluid Dynamics, Transport Phenomena, Electromagnetics to name a few. It has the capacity to perform all steps of a fluid flow simulation which include model building, mesh generation, data input, solution, and post processing.

When setting up the problem, care should be exercised when specifying the allowable errors for the solution convergence. Too large of an error allowance would result in false convergence, and too small of an allowable error would result in either a very lengthy calculation time or no convergence at all. The two main errors that are to be taken into consideration are the **Absolute Error** and the **Relative Error**. Absolute error is the difference between the true value and the approximation whereas relative error is the

ratio between absolute error and the true value. The absolute tolerance and relative tolerance are specified as 0.001 and 0.01 respectively in the FEMLAB code.

2.5 Mesh Sensitivity Analysis

To ensure the accuracy of the finite element solution, mesh sensitivity was performed. Mesh sensitivity is used to reduce the number of elements and nodes in the mesh while maintaining accurate results. This is done to minimize computational time and memory usage, while keeping a relatively accurate solution.

Mesh sensitivity analysis was made for the water - alcohol mixture (90:10 %) using the basic mesh (980 elements), refined mesh (3920 elements) and finer mesh (15680 elements). Figure 2.1 shows the default mesh size used in a time dependent solver used in FEMLAB. Figure 2.2 and 2.3 shows the variation of concentration and temperature respectively near the hot wall i.e at the point (1, 5). The mixture consisted of water – isopropanol (90:10 %).

The concentration of water near the hot wall was computed and compared with the results obtained by using consecutive finer meshes which had 3920 and 15680 elements respectively.The results obtained from using 980 elements mesh was compared with a mesh consisting 3920 elements. The error obtained was less than 0.0001 percent. Figure 2.2 shows the error between the values obtained by using the basic mesh (980 elements) and the finer mesh (15860 elements).

It can be observed that the basic mesh size with 980 elements can be used for the solving the model since the error was less than 0.01 %.

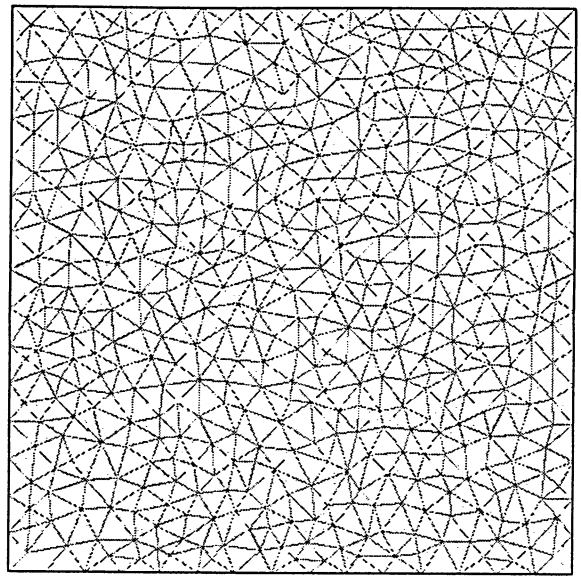

Figure 2.1: Triangular elements used in FEMLAB.

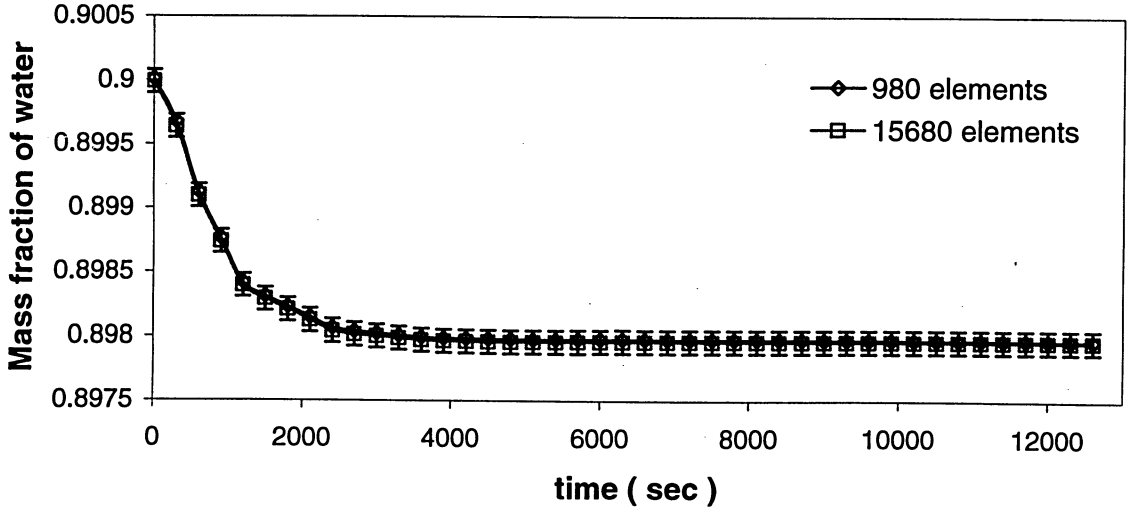

Figure 2.2: Percentage error in the mass fraction of water.

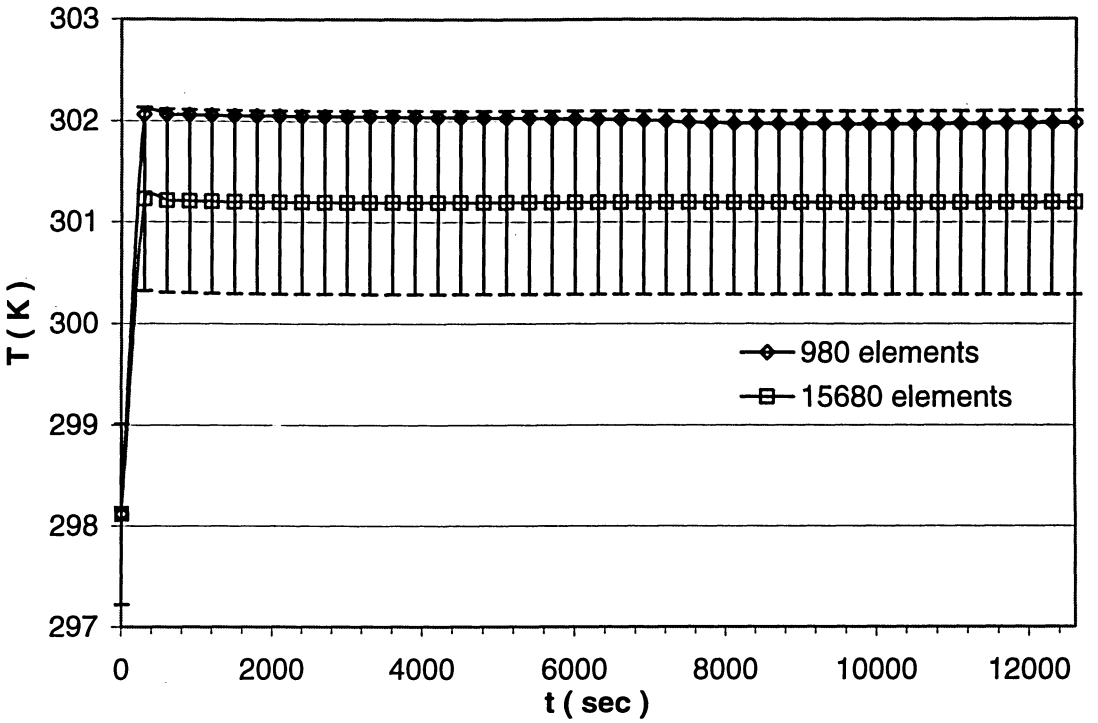

Figure 2.2: Percentage error in the temperature distribution.

CHAPTER 3

EFFECTS OF STATIC GRAVITY ON THE THERMAL DIFFUSION PROCESS IN BINARY MIXTURES

3.1 Introduction

Convection can be explained as the transfer of heat by the motion of or within fluid. Convection may arise from temperature differences either within the fluid or between the fluid and its boundary. The phenomenon in which convection is coupled to thermal and solute transport is known as double diffusion convection. Accurate descriptions of transport coefficients are needed for understanding and controlling processes. This requires a precise mathematical model as well as thorough knowledge of the transport coefficients.

The evaluation of transport coefficients by ground-based techniques is difficult due to the fact that buoyancy convection is very strong, which makes it difficult to accurately measure the thermal diffusion coefficient. One possible remedy to overcome this problem is to minimize the buoyancy by performing experiments in microgravity on free flying platforms, such as the International Space Station (ISS) and FOTON. Due to the absence of buoyancy-induced convection, experiments under such conditions may lead to accurate measurement of the Soret coefficient.

In this chapter the primary objective is to investigate the double diffusion convection of two binary mixtures in a square cavity and validate the results obtained by using the finite element method with the data reported by Chacha *et al* [1]. The two-dimensional numerical model is demonstrated for two binary mixtures of Methane-n-butane (20:80 wt %) and water-isopropanol (90:10 wt %) subject to the lateral heating condition and at various gravity levels. The influence of gravity induced convection on the thermal diffusion process is further discussed.

3.2 Mathematical Model

The mathematical formulation of the physical model under study is sketched in Figure 3.1. The system consists of a square cavity of side 10 mm containing a single-phase binary fluid mixture. The binary mixtures filling the cavity consist of two binary mixtures. They are water-isopropanol and methane-n-butane at a mass fraction of 90:10 wt% and 20:80 wt% respectively. The four walls are assumed to be non-reacting, rigid, impermeable, and with the no-slip condition. The two lateral walls are maintained at constant but different temperatures of T_{hot} and T_{cold} whereas the horizontal walls are assumed to be adiabatic.

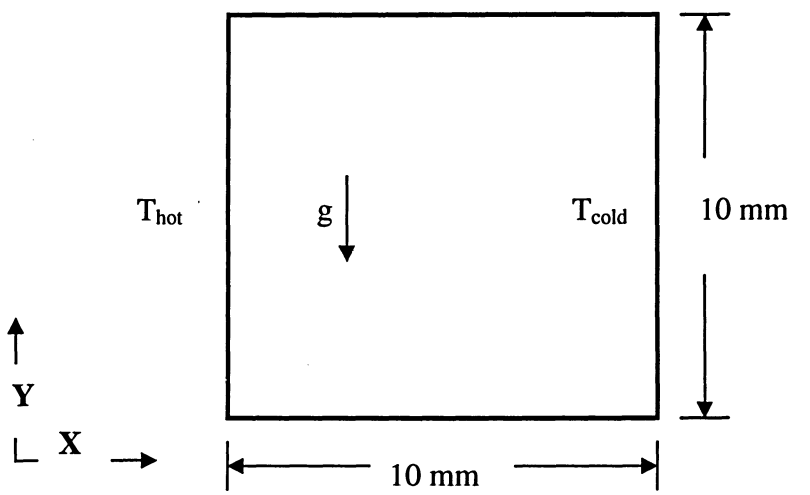

Figure 3.1: Two-dimensional model of the cavity.

3.3 Governing Equations

The governing equations for the problem described above are listed below:

3.3.1 Mass Conservation Equation

The conservation of mass can be expressed by the continuity equation in two dimensions as follows:

$$\nabla \cdot \vec{u} = 0 \tag{3.1}$$

where $\vec{u} = u \cdot \vec{i} + v \cdot \vec{j}$

Since the fluid is composed of two non-reacting species, the principle of mass conservation applies to each individual component as well as to the mixture as a whole. For each component and in terms of the mass fraction C, the principle of mass conservation in two-dimensions results in an equation of the form

$$\frac{\partial C}{\partial t} + u\frac{\partial C}{\partial x} + v\frac{\partial C}{\partial y} = \left(D_c \frac{\partial^2 C}{\partial x^2} + D_T \frac{\partial^2 T}{\partial x^2} \right) + \left(D_c \frac{\partial^2 C}{\partial y^2} + D_T \frac{\partial^2 T}{\partial y^2} \right) \tag{3.2}$$

3.3.2 Momentum Conservation Equation

The principle of momentum conservation is represented by the Navier–Stokes equations. For a two-dimensional case, momentum in x direction is given by

$$\rho\left(\frac{\partial u}{\partial t} + u\frac{\partial u}{\partial x} + v\frac{\partial u}{\partial y} \right) = -\frac{\partial p}{\partial x} + \mu\left(\frac{\partial^2 u}{\partial x^2} + \frac{\partial^2 u}{\partial y^2} \right) \tag{3.3}$$

whereas in the y direction the equation is given as

$$\rho\left(\frac{\partial v}{\partial t} + u\frac{\partial v}{\partial x} + v\frac{\partial v}{\partial y} \right) = -\frac{\partial p}{\partial y} + \mu\left(\frac{\partial^2 v}{\partial x^2} + \frac{\partial^2 v}{\partial y^2} \right) + f_y \tag{3.4}$$

where

$$f_y = -\rho \times g\left[1 - \beta_T (T - T_m) + \beta_c (C - C_o) \right] \tag{3.5}$$

where β_T and β_c are the thermal and concentration expansion coefficients respectively, T_m is the average temperature and C_0 in the initial concentration.

3.3.3 Energy Equation

Assuming that there is no internal heat generation, the principle of conservation of energy in two-dimensions is expressed by the following equation:

$$\rho\left(\frac{\partial T}{\partial t}+u\frac{\partial T}{\partial x}+v\frac{\partial T}{\partial y}\right)=\frac{k}{C_p}\left(\frac{\partial^2 T}{\partial x^2}+\frac{\partial^2 T}{\partial y^2}\right) \tag{3.6}$$

where k is the thermal conductivity and C_P is the specific heat at constant pressure.

3.4 Boundary and Initial Conditions

Velocity boundary conditions:

The no-flow and no-slip boundary conditions are considered on the walls

$$\begin{aligned} u = v = 0, \text{ at } x = 0,\ x = 10 \text{ mm} \\ u = v = 0, \text{ at } y = 0,\ y = 10 \text{ mm} \end{aligned} \tag{3.7}$$

Species boundary conditions:

These are not subject to surface reactions or mass flux

$$\begin{aligned} D_c\frac{\partial C_i}{\partial x}+D_T\frac{\partial T}{\partial x}=0,\ x = 0,\ x = 10 \text{ mm} \\ D_c\frac{\partial C_i}{\partial y}+D_T\frac{\partial T}{\partial y}=0,\ y = 0,\ y = 10 \text{ mm} \end{aligned} \tag{3.8}$$

The vertical walls are subject to constant temperature boundary conditions (Dirichlet conditions). The other two walls are assumed to be adiabatic. $\frac{\partial T}{\partial y}=0$

For methane-n-butane mixture

$$\begin{aligned} &T = 338\ K,\ x = 0 \\ &T = 328\ K,\ x = 10\ mm \end{aligned} \tag{3.9}$$

For water-isopropanol mixture

$$\begin{aligned} &T = 303\ K,\ x = 0 \\ &T = 293\ K,\ x = 10\ mm \end{aligned} \tag{3.10}$$

Initial conditions:

The initial conditions are as follows:

$$\begin{aligned} &u(x,y) = v(x,y) = 0, \\ &p(x,y) = p_o, \\ &C(x,y) = C_o, \\ &T(x,y) = T_o \end{aligned} \tag{3.11}$$

The physical properties of the two binary mixtures are given in Table 3.1 and 3.2.

Table 3.1: Physical properties of Methane-n-Butane (20:80 wt %) @ 60^{0}C, P_0 = 35 MPa

Average density of the mixture ρ_0 at 60°C	452.092 kg/m^3
Initial composition of methane c_0	0.2
Thermal expansion coefficient β_T	2.0849×10^{-3} 1/K
Volumetric concentration expansion coefficient β_C	0.71489
Molecular diffusion coefficient D_c	0.4333×10^{-8} m^2/s
Thermal diffusion coefficient D_T	-4.55×10^{-12} m^2/s.K
Dynamic viscosity of the mixture η at 60°C	7×10^{-5} Pa.s
Specific heat c_p	2040 J/ (kg K)
Thermal conductivity k	0.095 W/ (m K)

Table 3.2: Physical properties of Water-Isopropanol (90:10%) @ $T_0 = 20^0C$, $P_0 = 1bar$

Average density of the mixture ρ_0 at 20°C	984 kg/m^3
Initial composition of water c_0	0.9
Thermal expansion coefficient β_T	3.1×10^{-4} 1/K
Volumetric concentration expansion coefficient β_C	0.1386
Molecular diffusion coefficient D_c	8.7×10^{-10} m^2/s
Soret coefficient S_T	-10.6×10^{-3} 1/K at 21°C -7.63×10^{-3} 1/K at 37.5°C
Kinetic viscosity of the mixture ν at 20°C	1.41×10^{-6} m^2/s
Specific heat c_p	3990.5 J/ (kg K)
Thermal conductivity k	0.522 W/ (m K)

3.5 Results and Discussion

The full transient Navier-Stokes equations, coupled with energy and mass transfer equations along with the boundary conditions from (3.1) to (3.8) were solved numerically using the Galerkin'sFinite Element Method. The study consisted of two cases: Case1: Methane – n-Butane mixture and Case 2: Water – Isopropanol mixture subject to different static gravity conditions. The different static gravity conditions applied are: (1) $g = 10^{-2}\, g_0$, (2) $g = 10^{-3}\, g_0$, (3) $g = 10^{-4}\, g_0$ and (4) $g = 10^{-6}\, g_0$. The results obtained by numerical simulation are discussed below.

3.5.1 Case 1: Methane – n-Butane Mixture

The fluid cavity filled with methane-n-butane at 20:80 wt % is subject to different static gravity conditions. All the figures given here show the variation of concentration and temperature in the middle of the cavity along the x direction, (x, 5 mm). This binary mixture is investigated under different levels of gravity when the two lateral walls are

maintained at different yet constant temperatures such that the temperature difference is 10 K. The top and bottom walls are assumed to be adiabatic.

Figure 3.2 presents the variation of methane concentration for 10^{-2} g_0 in the horizontal direction within the cavity. At this level, the effect of buoyancy convection is more prominent. It causes a strong single cell clockwise flow in the cavity with velocities in the order of 10^{-5} m/s; see Figure 3.8(d). A major component separation takes place along the direction of the temperature gradient in the vicinity of the hot and cold walls; whereas a homogenous mass distribution is found in the centre of the cavity. It can be observed that a boundary layer is formed near the hot and cold walls; see Figure 3.8(a). The thickness of the boundary layers was found to be about 1 mm. The comparison of results with Chacha *et al.* [1] showed that the error was less than 1%.

In Figure 3.2 the variation of concentration near the hot and cold walls shown by the sharp curve before becoming uniform can be explained by the fact that it is the transitional region because the walls are assumed to be at no slip condition and there is a strong convection in the middle of the cavity.

Figure 3.3 displays the temperature profile in the cavity at 10^{-2} gravity level. The temperature profile is completely distorted in this case. A sharp increase and a sharp decrease in temperature can be observed near the hot and the cold walls respectively whereas the temperature remains equal to its mean value in the central and very large portion of the cavity. The significant horizontal temperature gradient observed near the vertical walls can be explained due to the strong buoyancy convection. .

Figure 3.4 presents the variation of mass fraction of methane inside the cavity at 10^{-3} g_0 level. It can be observed that the boundary layers near the both walls starts to disappear gradually. This can be explained due to the fact that the magnitude of gravity decreases which in turn reduces the buoyancy effects. The concentration contour in Figure 8(b) clearly shows this phenomenon.

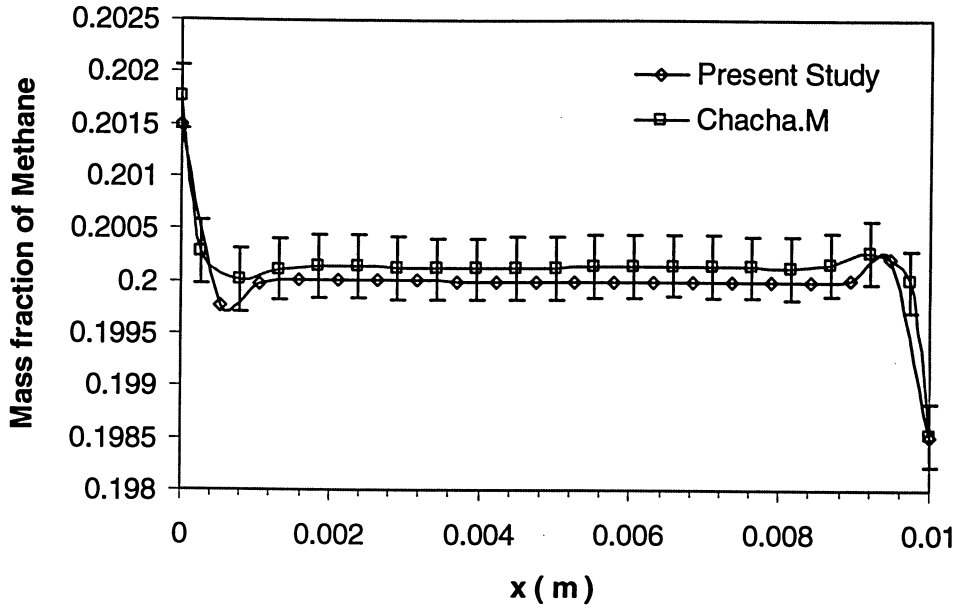

Figure 3.2: Horizontal variation of mass fraction of Methane at $g = 10^{-2} g_0$.

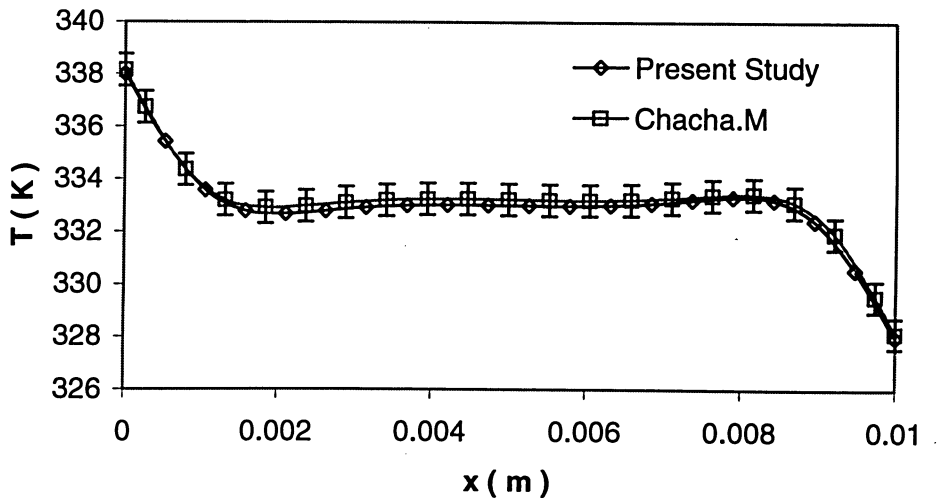

Figure 3.3: Horizontal variation of Temperature, $g = 10^{-2} g_0$.

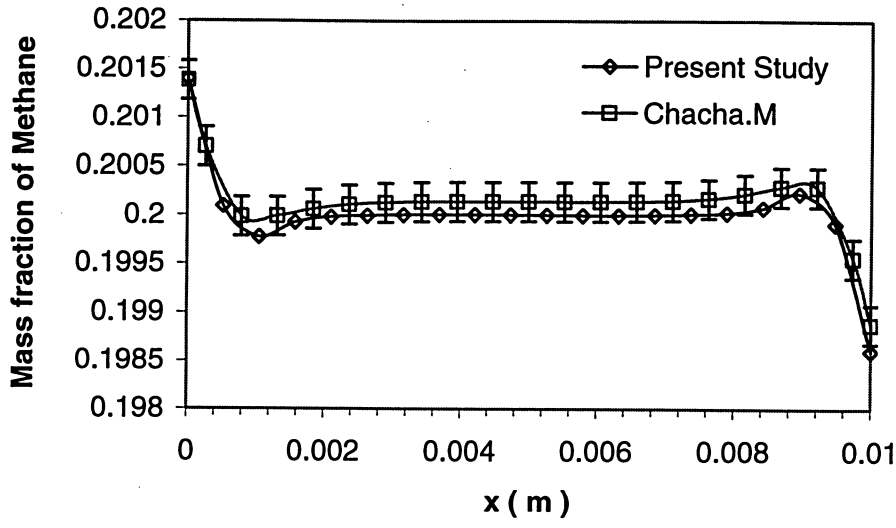

Figure 3.4: Variation of mass fraction of methane, $g = 10^{-3}\ g_0$.

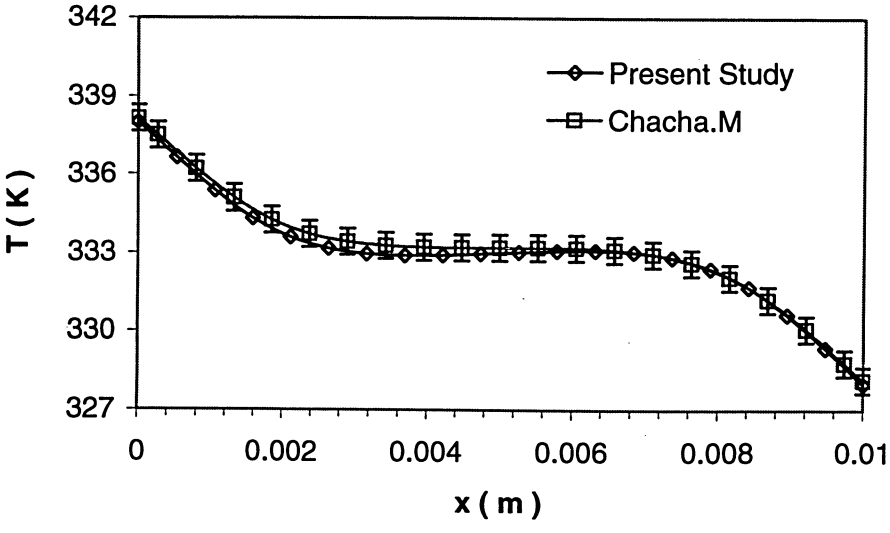

Figure 3.5: Horizontal variation of Temperature, $g = 10^{-3}\ g_0$.

Figure 3.5 displays the temperature profile within the cavity at 10^{-3} g_0 condition. The temperature profile in this case tends to smoothen up instead of being distorted as seen in the 10^{-2} g_0 case. It can also be noted that the sharp curves near the hot and cold walls start to elongate gradually. The difference was found to be less than 1% when the results were compared with Chacha *et al* [1].

Figure 3.6 displays the mass fraction variation of methane at $g = 10^{-6}$ g_0 condition. Methane mass fraction gradually decreases from the hot wall towards the cold wall. The mass variation follows an almost linear pattern. The concentration contour given in Figure 3.8(c) gives a clear picture of the almost linear variation of the methane concentration. This can be explained by the fact that as the magnitude of gravity approaches zero gravity level the concentration as well as temperature profile tends to follow the zero gravity patterns. Figure 3.7 depicts the temperature profile and it can be noted that the variation of temperature profile is linear.

Figure 3.9 compares the concentration variation of methane within the cavity for different gravity levels. For the 10^{-2} g_0 case, a boundary layer is developed near the hot and cold walls. Methane tends to move towards the hot wall; whereas n-butane moves towards the cold wall. This is due to the fact that methane is lighter than n-butane. At 10^{-3} g_0 level the boundary layers near the walls start to smoothen up and tend to follow the linear pattern. At microgravity level, 10^{-6} g_0, the phenomenon tends to follows the zero gravity patterns. This can be explained by low magnitude of applied gravity level, i.e. it approaches the zero gravity level.

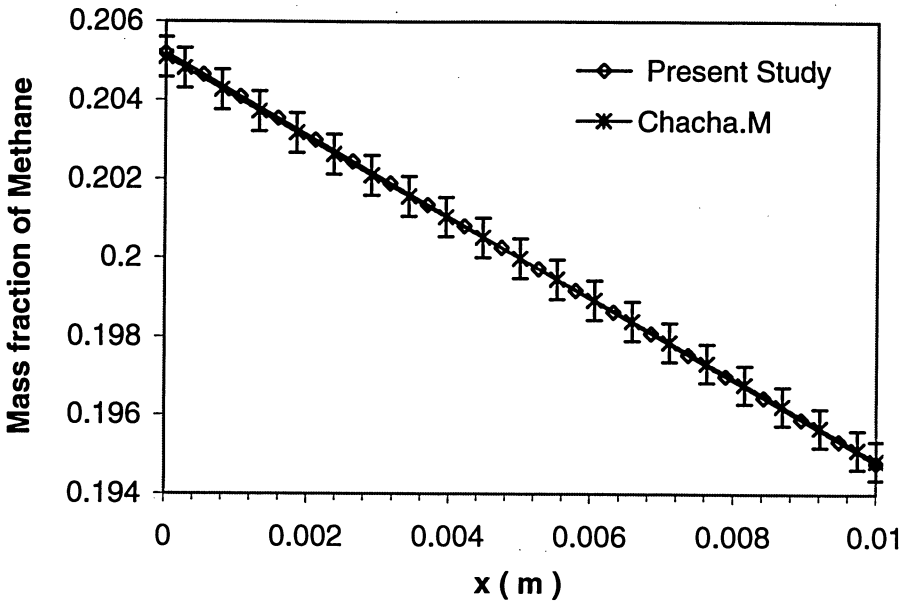

Figure 3.6: Variation of mass fraction of methane, $g = 10^{-6}\, g_0$.

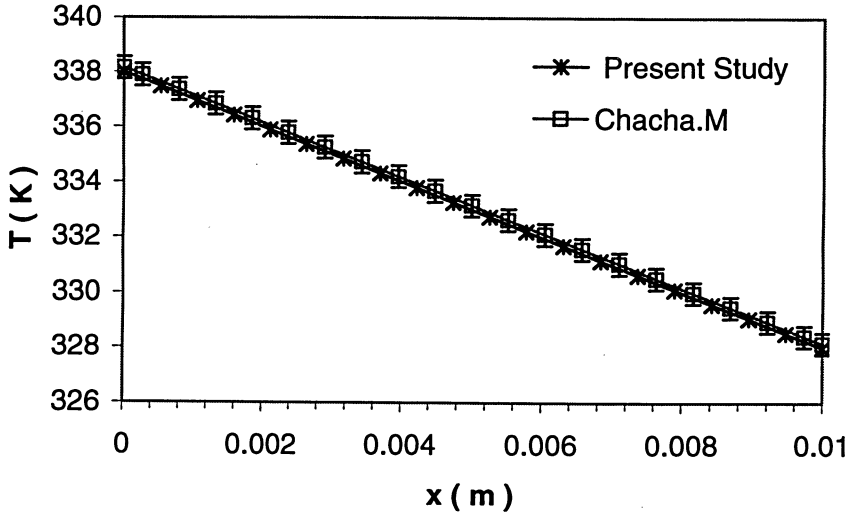

Figure 3.7: Horizontal variation of Temperature, $g = 10^{-6}\, g_0$.

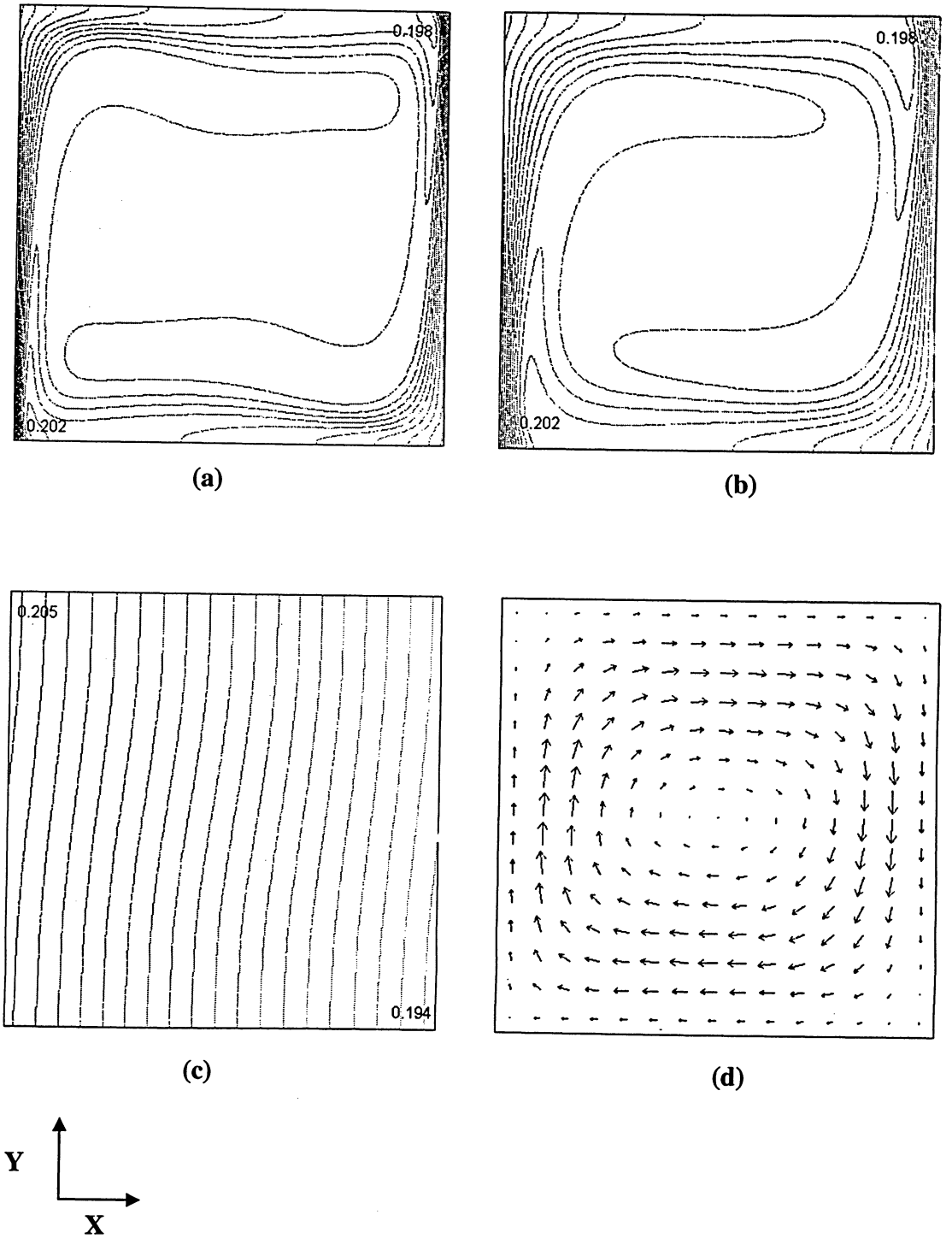

Figure 3.8: Concentration contours (ΔC) of methane at different gravity levels,

(a) $g = 10^{-2} g_0$, (b) $g = 10^{-3} g_0$, (c) $g = 10^{-6} g_0$, (d) velocity vector within the cavity.

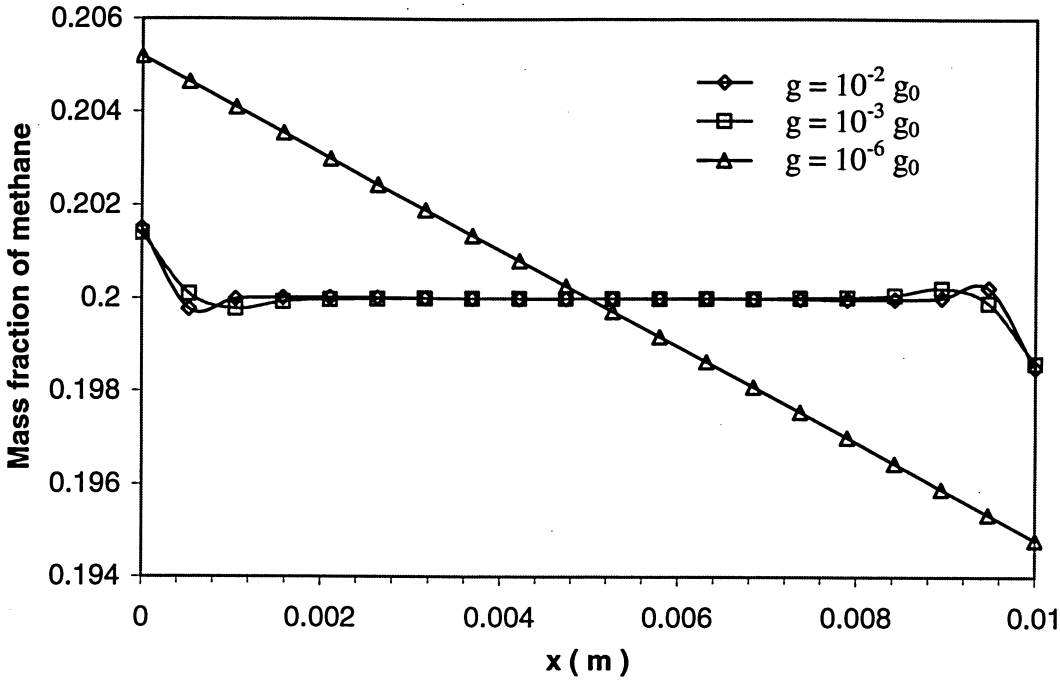

Figure 3.9: Comparison of concentration profiles under different levels of gravities.

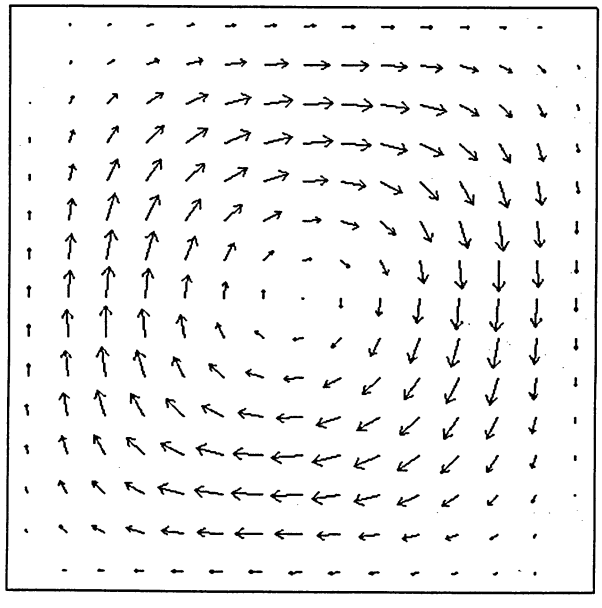

Figure 3.10: Velocity vector within the cavity.

3.5.2 Case 2: Water – Isopropanol Mixture

In this case the fluid cavity is filled with the binary mixture consisting of water-isopropanol at 90:10 wt % and is subject to different static gravity conditions. The governing equations and the numerical solution are the same as the methane-n-butane mixture case. Similar pattern can be found with this mixture as Case 1; hence the results are discussed briefly.

Figure 3.11 (a) shows the concentration contours of water under zero gravity level. In zero gravity conditions the concentration is distributed linearly along the width of the cavity. This linear variation shows that at zero gravity level, the Soret effect is dominant; buoyancy force is absent, which in turn causes separation in the mixture. Figure 3.12 (a) shows the temperature contours within the cavity. It can be seen that the temperature varies linearly along the width of the cavity. This can be explained due to the absence of buoyancy under zero gravity condition.

Figure 3.11 (b) presents the concentration contours of water for the gravity level of 10^{-2} g_0. At this level, the effect of buoyancy convection is more prominent. It causes a strong single cell clockwise flow in the cavity with velocities in the order of 10^{-5} m/s; see Fig 3.10. A major component separation takes place along the direction of the temperature gradient in the vicinity of the hot and cold walls; whereas a homogenous mass distribution is found in the centre of the cavity. The lighter component, isopropanol, tends to move towards the cold wall, whereas the heavier component water moves towards the cold wall due to the negative Soret effect. This phenomenon is very different from what was observed in the case of zero gravity condition where the concentration profile was linear. The thickness of the boundary layers is around 1.1 mm. The deviation from zero gravity is also evident in the temperature profile. Figure 3.12 (b) presents the temperature contours within the cavity at 10^{-2} g_0 level. The temperature profile is distorted due to the buoyancy force.

Figure 3.11 (c) displays the concentration distribution of water in the cavity under 10^{-4} g_0 level. The concentration profile tends to become linear and it can also be noted that the boundary layers near the hot and cold walls have disappeared. Figure 3.12 (c) shows the temperature contour where the distortion has been greatly reduced in this case of 10^{-4} g_0 gravity.

Figure 3.11 (d) shows the water concentration contours inside the cavity for the microgravity case ($g = 10^{-6}$ g_0). It can be seen that there is an almost linear variation in the concentration as it decreases from the hot wall towards the cold wall. This phenomenon follows the similar pattern as the zero gravity condition, where there is very small buoyancy and hence the variation of concentration which is almost linear. Same is the case for temperature profile; see Figure 3.12 (d); it follows the similar fashion as the zero gravity case.

Figure 3.13 compares the behaviour of the concentration of water within the cavity for different levels of gravity. At zero gravity both concentration as well as the temperature profiles are linear. This can be explained due to the absence of buoyancy force. For the 10^{-2} g_0 case, a boundary layer is developed near the hot and cold walls. Due to negative Soret effect isopropanol tends to move towards the cold wall, whereas water moves towards the hot wall. At 10^{-4} g_0 the boundary layers near the walls start to disappear and tend to become linear. At microgravity level, 10^{-6} g_0, the phenomenon follows the zero gravity patterns. This can be explained by low magnitude of applied gravity level, i.e. it approaches the zero gravity level. In all the above cases the results obtained by using FEM appears to be in good agreement with the data reported by Yan *et al* [32], with error less than 2% for most of the times.

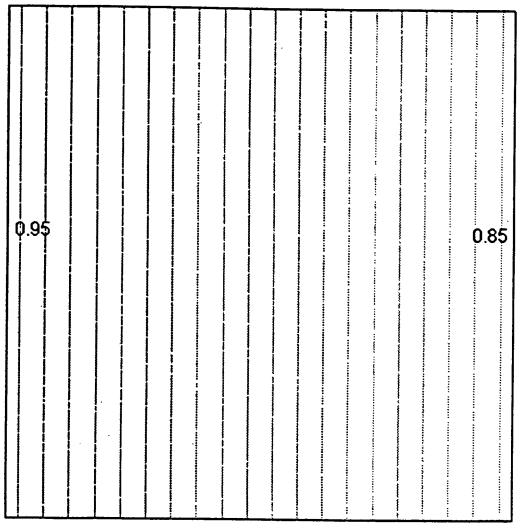

(a) $g = 0$

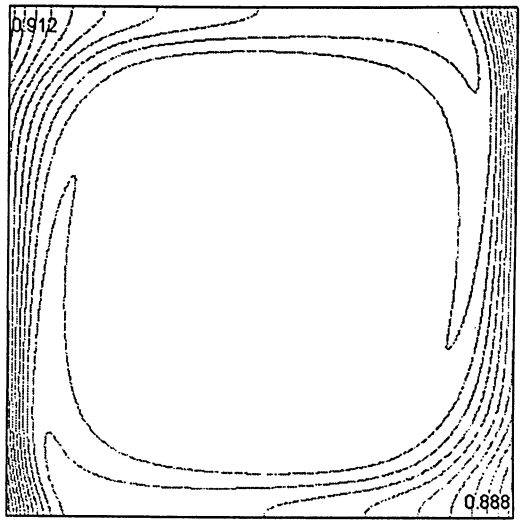

(b) $g = 10^{-2} g_0$

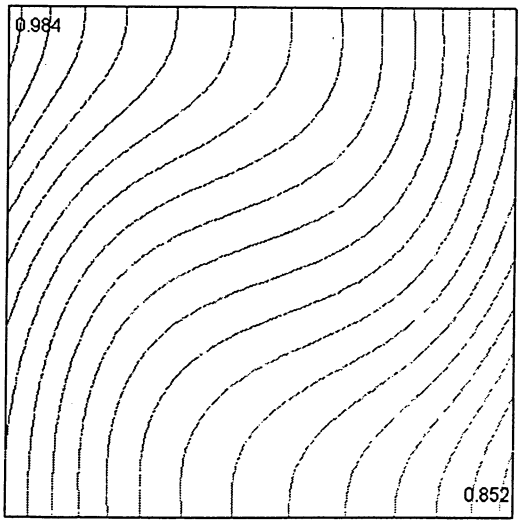

(c) $g = 10^{-4} g_0$

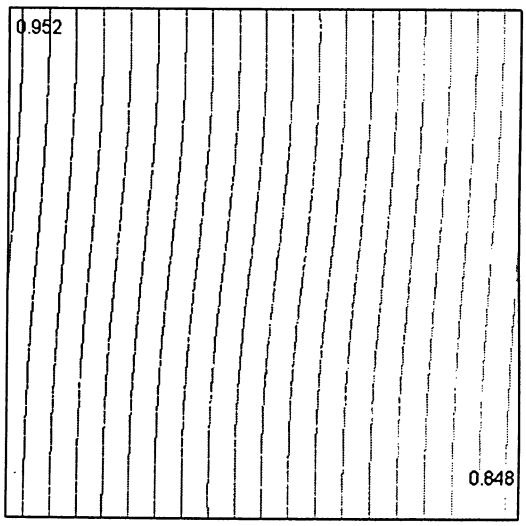

(d) $g = 10^{-6} g_0$

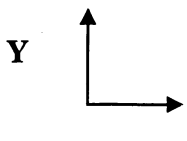

Figure 3.11: Concentration contours (ΔC) of water at different gravity levels.

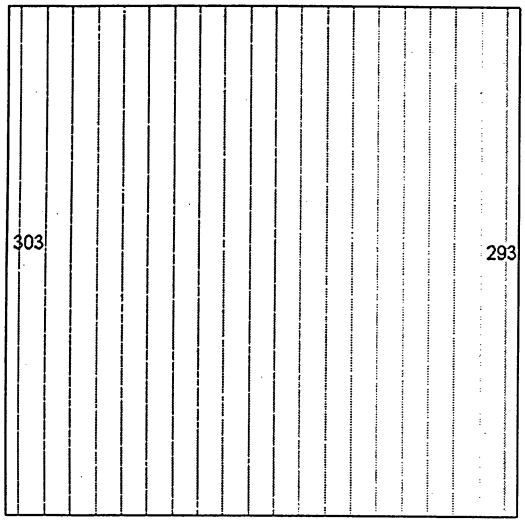

(a) $g = 0$

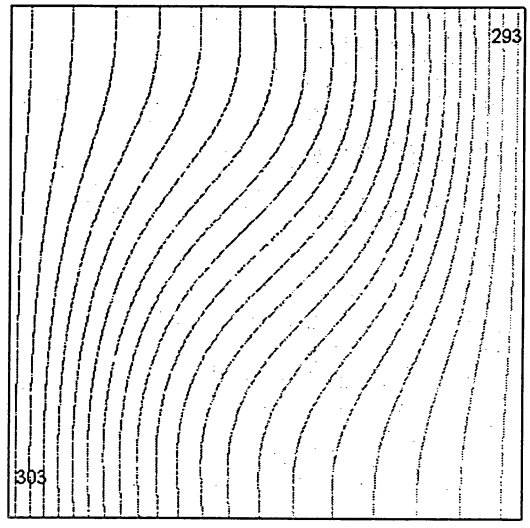

(b) $g = 10^{-2}\, g_0$

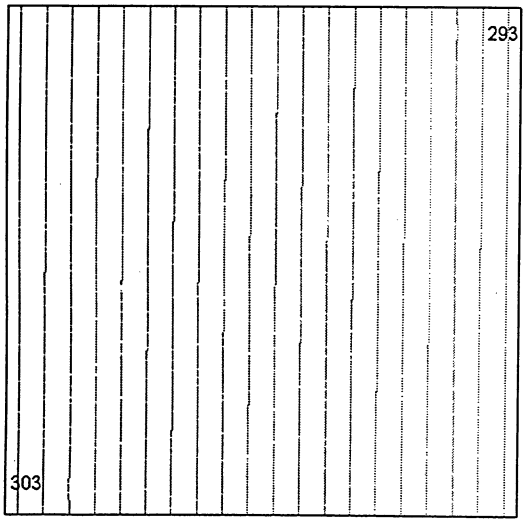

(c) $g = 10^{-4}\, g_0$

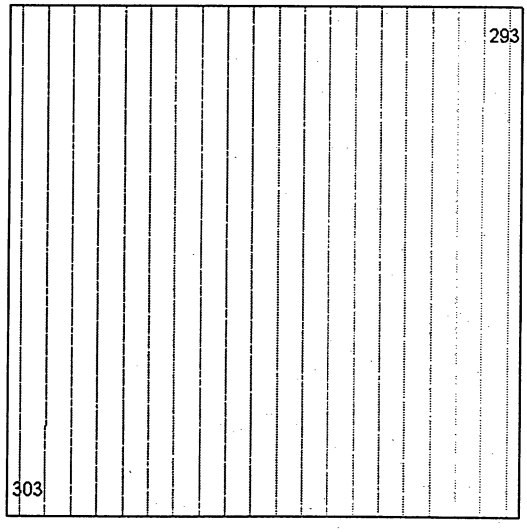

(d) $g = 10^{-6}\, g_0$

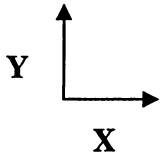

Figure 3.12: Temperature contours (ΔT) at different gravity levels.

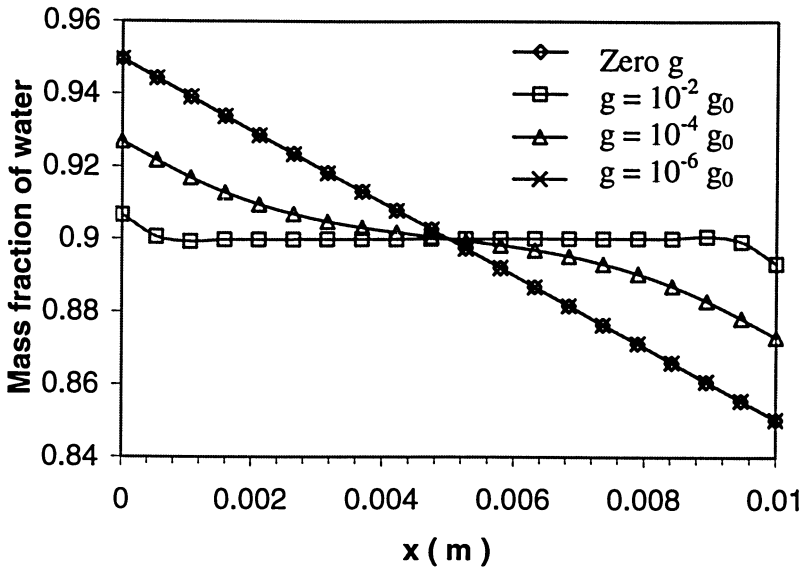

Figure 3.13: Comparison of concentration profiles under different levels of gravities.

3.6 Summary

In this chapter the effects of different gravity levels on the thermal diffusion process in two single phase binary mixtures were studied. The binary mixtures consisted of methane-n-butane (20:80 wt %) and water-isopropanol (90:10 wt %). In the analysis, component concentration profiles, temperature profiles and velocity in the cavity were used to investigate the effect of different gravity levels on the thermal diffusion phenomena. The analysis revealed a consistent behaviour between the two binary mixtures. From the results obtained, it could be inferred that the Finite Element Method gives good results for both hydrocarbon as well as water – alcohol mixtures. Furthermore, it can be concluded that the effects of the static gravity on thermal diffusion were very significant and buoyancy convection plays an important role in the species separation. Also, the results in this study were found to be in good agreement with the data reported by Chacha *et al.* [1] and Yan *et al.* [32].

CHAPTER 4

EFFECTS OF G-JITTERS ON THERMAL DIFFUSION PROCESS IN BINARY MIXTURES

4.1 Introduction

The thermal diffusion process, also known as the Soret effect is the phenomenon in which the components of an initially homogenous mixture tend to separate from each other when a temperature gradient is applied. For binary mixtures, this is measured by the Soret coefficient, S_T, the ratio of the thermal diffusion coefficient, D_T, to the molecular diffusion coefficient, D_c. Great efforts has been made to model or experimentally investigate this process due to the importance of the Soret effect on various applications such as the study of compositional variation in hydrocarbon reservoirs, hydrodynamic instability of mixtures, mineral migrations and mass transport in living matter to name a few.

Convection has a major influence on the accuracy of the Soret measurements. On earth, the buoyancy convection is very strong, which makes it nearly impossible to accurately measure the thermal diffusion coefficient. The microgravity environment minimizes the effect of the gravity and allows the true diffusion limit to be achieved. Therefore nowadays performing diffusion experiments in the space appears to be a promising and feasible option. However, virtually all space laboratories experience static and/or oscillatory residual accelerations called g-jitter due to the movement of the crew, aerodynamic forces, gravity gradient, solar pressure, thruster firing for altitude adjustment, operation of equipment on board, servicing activities, docking / berthing etc. G-jitters have a wide spectrum of amplitudes and frequencies. The existence of the g-jitter does induce a convection motion and affect the accuracy of the measurement. Hence, it is important to analyze the effect of the g-jitter on diffusion processes for understanding the space experiments and the measurement results from the space laboratories better.

This chapter numerically investigates the effects of different g-jitter cases with respect to the amplitude as well as static residual gravity cases on the thermal diffusion process in a fluid mixture of water-isopropanol (90:10 wt %) within a square cavity. The full transient Navier-Stokes equations with Boussinesq approximation, coupled with energy and mass transfer equations were solved numerically using the Finite Element Method.

4.2 Mathematical Model

The physical geometry of the square cavity is the same as discussed in Chapter 3; see Figure 3.1. A lateral heating condition is applied to the cavity with temperatures of the hot and cold walls equal to 303K and 293K, respectively. All other walls are assumed to be thermally insulated, rigid and impermeable to matter. The system is subject to vibrations due to the oscillating components of the gravity vector, which is oriented perpendicular to the temperature gradient, i.e., in the Y direction. The physical properties of the mixture used in the simulation are summarized in Table 3.2. Both D_c and D_T are assumed to be constant in the simulation.

4.2.1 Governing Equations

The governing equations are the same from (3.1) to (3.6) as discussed in Chapter 3, except the gravity term (g) in the body force term, given by equation (3.5). For this case, gravity term 'g' is given by the summation of two components (i) static or steady gravity and (ii) vibrations or g-jitter. The body force term in the momentum equation is given by [1]

$$f_y = -\rho \times g(t)\left[1-\beta_T (T-T_m)+\beta_C (C-C_0)\right] \tag{4.1}$$

here g(t) is given by

$$g(t) = g_{st} + g_{vib} \tag{4.2}$$

where g_{vib} is given by

$$g_{vib} = g_0 \mathrm{Sin}(2\pi ft) \tag{4.3}$$

where f is the frequency of vibrations in Hz and t is the time (sec)

4.3 Results and Discussion

Four cases with different levels of residual and oscillatory gravities have been modeled. They are:

Table 4.1 Different levels of residual and oscillatory gravities considered

Case	Static gravity (g_{st})	Vibration gravity (g_{vib})
1	0	10^{-3} g_0 Sin ($2\pi ft$)
2	10^{-4} g_0	0
3	10^{-4} g_0	10^{-3} g_0 Sin ($2\pi ft$)
4	10^{-4} g_0	10^{-4} g_0 Sin ($2\pi ft$)

Results obtained from the four cases are discussed below.

4.3.1 Effects of pure oscillatory g-jitters - Case 1

This case represents the situation where the static gravity component is absent, only pure sinusoidal vibration is present. The frequency of oscillation is 0.025 Hz. Figure 4.1 compares the concentration variation of water in case 1 with zero gravity level. The variation is shown along the X direction in the middle of the cavity, (x, y = 5 mm). The distribution of water has a tendency to approach the linear line as seen at the zero gravity level and when reaching the steady state. This implies that in terms of the component

distribution the system is very possible to follow a similar fashion as the zero gravity level if sufficient time is given.

Figure 4.2 presents the concentration variation of water along the centre of the cavity at various time steps. It can be noted that as time prolongs, the concentration profile tends to reach the linear pattern as seen in the zero gravity case. This may be explained as time proceeds, the oscillating components cancel out the effect in opposite directions. This can be further verified by examining the temperature profile. Figure 4.3 shows the temperature profile, which illustrates the variation of temperature in the X direction along the middle of the cavity. The linear temperature profile observed in zero gravity is also shown here as a comparison. It can be noted that the temperature profile follows the similar pattern as seen in the zero gravity case; see Figure 4.3.

In Case 1, the velocity profile is symmetric to the X axis and changes in a sinusoidal wave fashion. The amplitude of oscillation is found to be in the order of 10^{-6} m/s; see Figure 4.4. Figure 4.5 (a) and (b) present the concentration and temperature contours respectively, within the cavity for Case1. It can be seen from the contours that both the concentration and temperature show slight distortions.

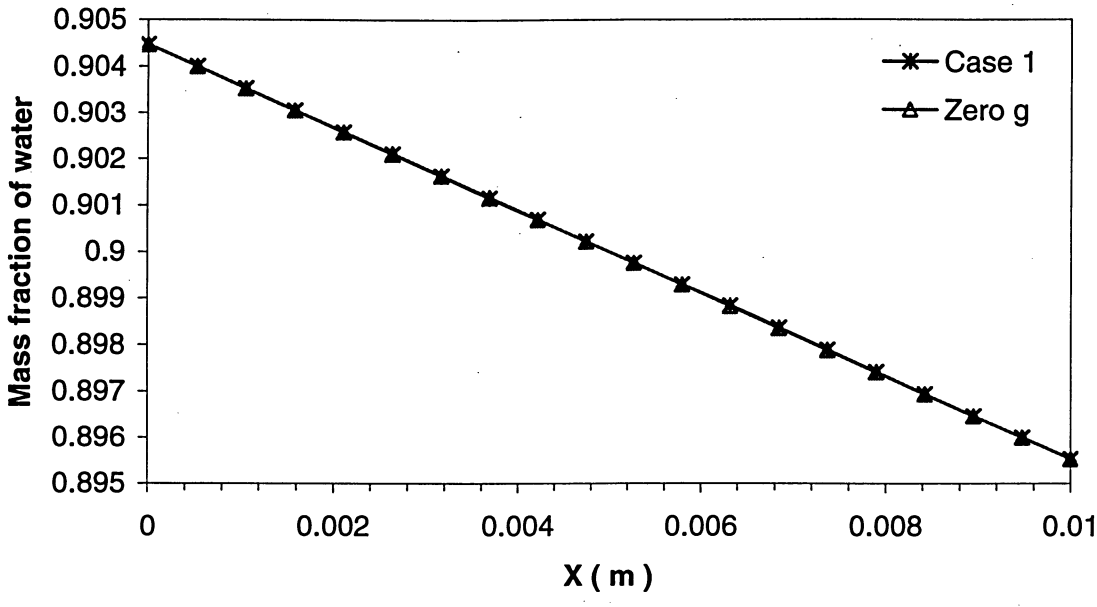

Figure 4.1: Comparison of water concentration at the middle of the cavity.

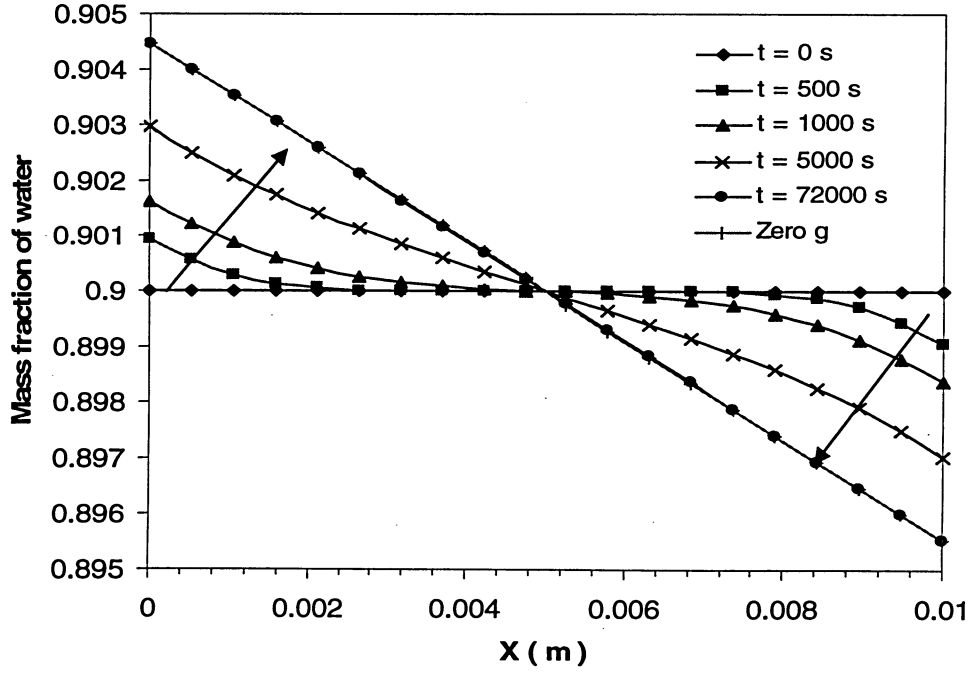

Figure 4.2: Comparison of water concentration at various time steps.

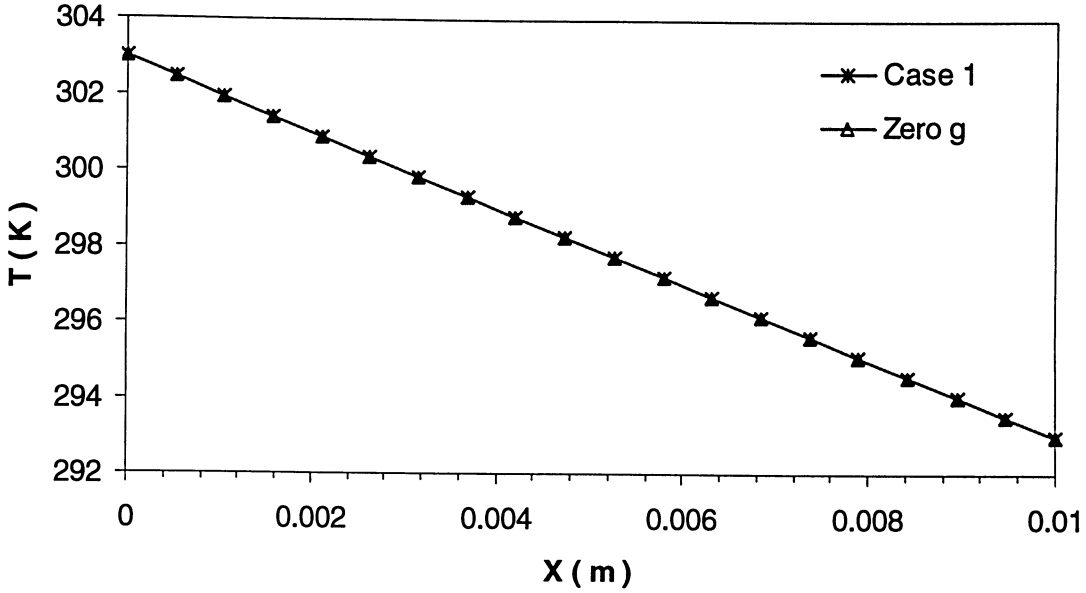

Figure 4.3: Comparison of temperature distribution with zero gravity level.

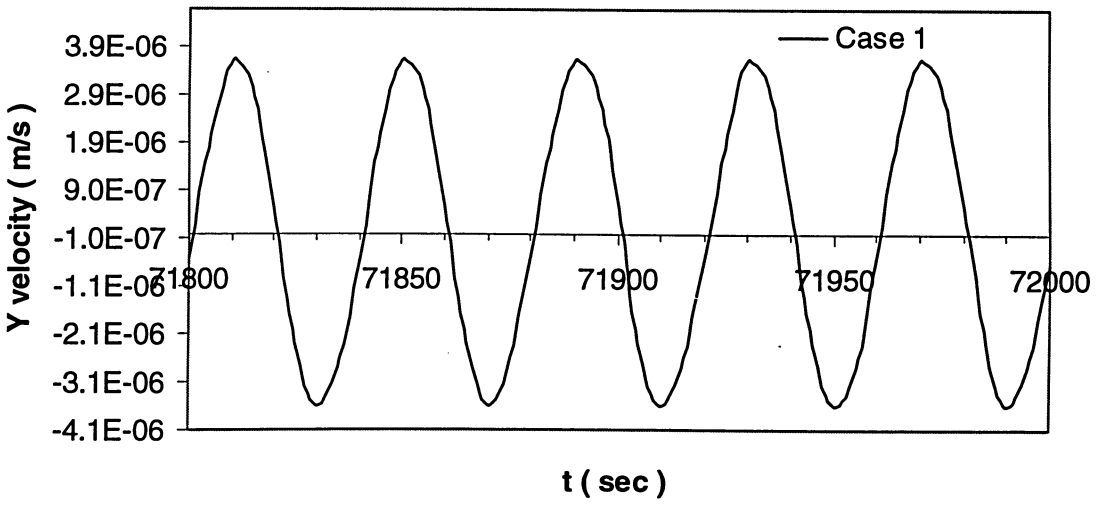

Figure 4.4: Velocity profile in the y direction for the last few time steps.

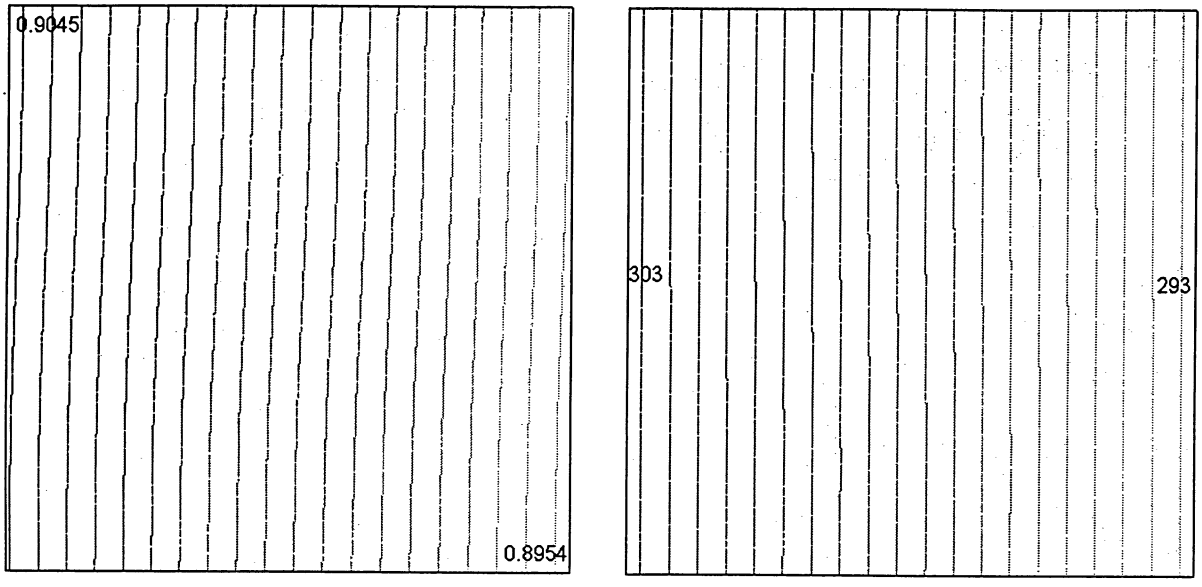

Figure 4.5: (a) Concentration contour (ΔC), (b) Temperature contour (ΔT) for case 1.

4.3.2 Effect of static residual gravities – Case 2

The effects of static gravities on fluid diffusion are discussed in detail in Chapter 3; a brief summary is given here. When just the static residual gravity is present, the buoyancy force acts constantly on the mixture without changing direction. The magnitude of the residual gravity determines the degree of its negative effect on thermal diffusion process. Figure 4.6 compares the water distribution contours in the cavity at different levels of residual gravity. The lighter component, isopropanol, tends to move towards the cold wall, whereas the heavier component water moves towards the cold wall due to the negative Soret effect.

At zero gravity level, the concentration of water is distributed linearly along the direction of the temperature gradient from the hot wall to the cold wall; see Figure 4.6 (a). There is only a slight change in concentration profile at $10^{-6}g_0$ level when compared to the linear pattern of zero gravity; see Figure 4.6 (d) When the gravity level is increased further, the

effect of buoyancy convection becomes more significant. The smooth and linear concentration profile gets distorted greatly at $10^{-4}g_0$; see Figure 4.6 (c).

A boundary layer structure is formed in the concentration profile when the gravity is increased to $10^{-2}\,g_0$; see Figure 4.6 (b). It is formed along the direction of the temperature gradient. Mass separation takes place mainly in the vicinity of the hot and cold walls; whereas in the centre of the cavity it is almost homogenous. The thickness of the boundary layers is found to be about 1 mm. This may be explained by the fact that the residual gravity initiates a mixing in the cavity due to the effect of the buoyancy force. As the magnitude of the residual gravity is increased further towards ground gravity level, such mixing becomes very dramatic and the boundary layer structure becomes more prominent.

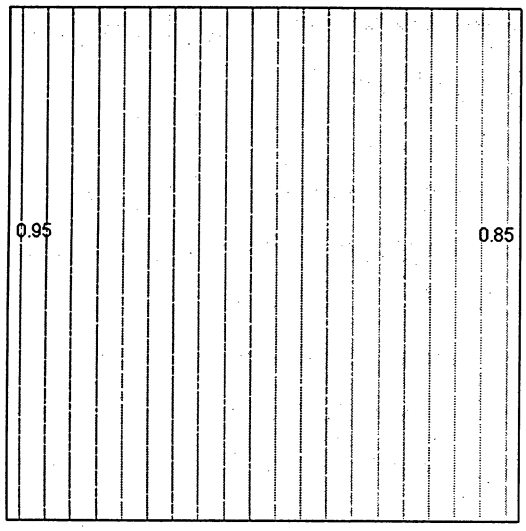

(a) $g = 0$

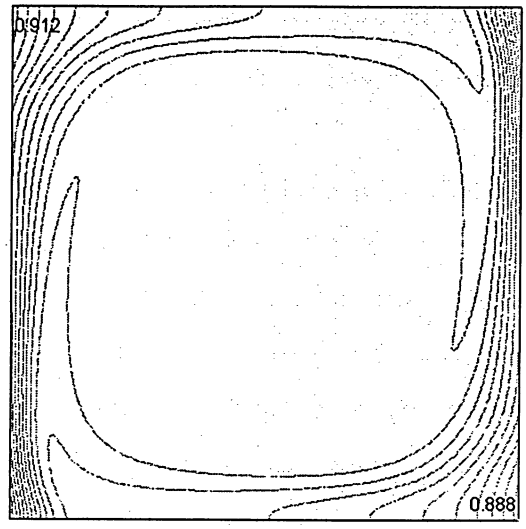

(b) $g = 10^{-2}\ g_0$

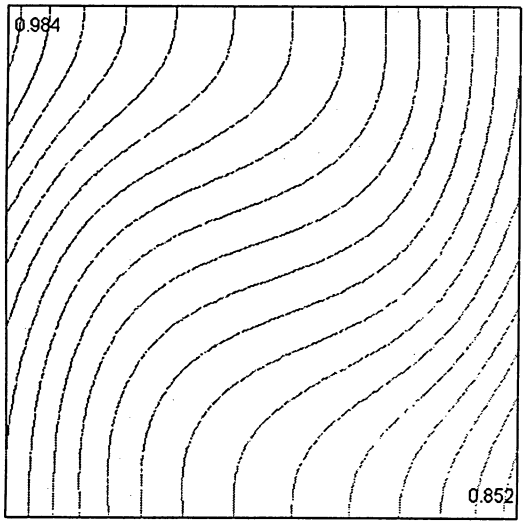

(c) $g = 10^{-4}\ g_0$

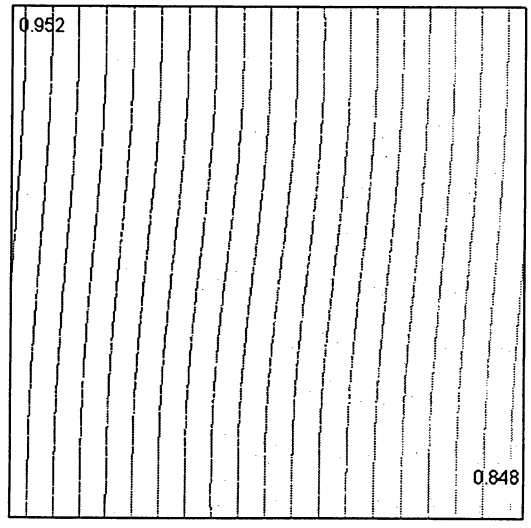

(d) $g = 10^{-6}\ g_0$

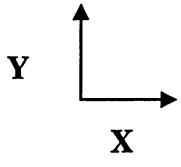

Figure 4.6: Concentration contours of water at different gravity levels.

4.3.3 Effect of combined static and oscillatory g-jitters – Case 3 and Case 4

In real time situations, g-jitters are random and may consist of both static and oscillatory components simultaneously. To better understand the fluid diffusion behaviors under these conditions, Case 3 and Case 4 were simulated, as mentioned earlier. In both cases, the magnitude of the static component of the g-jitters remains at 10^{-4} g_0; whereas the magnitudes of the oscillatory component are kept at 10^{-3} g_0 and 10^{-4} g_0.

With the addition of a non-zero static residual gravity, the buoyancy convection will become much stronger than the one induced by pure oscillatory gravities alone. First of all, such changes will be reflected in the local velocity profile, see Figure 4.7. When only the oscillatory g-jitter is present, as in Case 1, the velocity is symmetric to the X axis and changes in a sinusoidal shape. However, in the case of combined static and oscillatory gravities, for example in Case 3, the mean value of the velocity plot is not equal to zero. In addition, the amplitude of the velocity oscillation increases significantly compared to that in Case 1, which is pure oscillatory gravity condition.

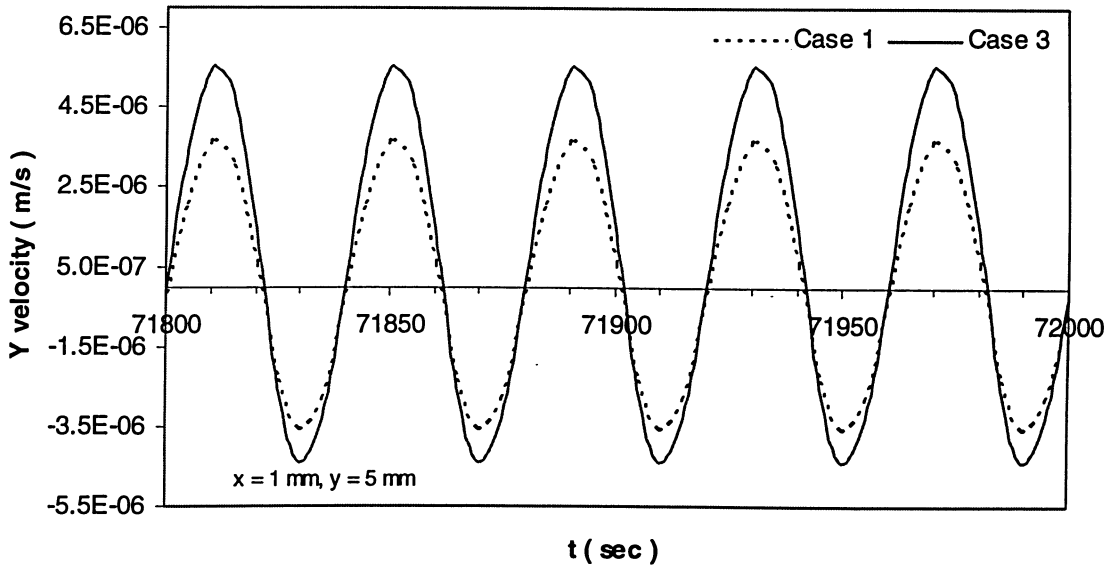

Figure 4.7: Comparison of velocity variation with time at the point (1, 5) for case 1 and 3 (last few time steps).

Figure 4.8 compares the water concentration contours of Case 3 and Case 4 with their corresponding static gravity case ($g_{st} = 10^{-4}g_0$). It can be noted that with the presence of the oscillatory g-jitter component, the water distribution has been further distorted compared to that when only the static residual gravity exists. This may be explained by the presence of oscillatory component of the g-jitter which causes the vibrational convection. An extra disturbance is induced by the vibrational convection on the fluid flow in addition to that caused by the static residual gravity. Thus the Soret separation is affected by the combined effect of both static and oscillatory gravities.

Figure 4.9 compares the water concentration along the X axis for different g-jitter cases. Figure 4.10 presents the time variation of water concentration near the hot wall for case 1 and figure 4.11 gives the concentration variation for the last few time steps. If we look the last time steps, we can see that there is a strong vibrational convection. It can be inferred that the convection contributed by the static gravity is the same; this can be explained as the result of different levels of vibrational convections attributing to the oscillatory part of g-jitters. The fact that the concentration contour is distorted much significantly indicates a stronger vibrational convection generated by the oscillatory component of g-jitters. One should be reminded that the same tendency has also been observed at the pure oscillatory g-jitter case, by which it may be concluded that g-jitters have a much harmful effect on diffusion process regardless of the existence and/or the magnitude of static residual gravities.

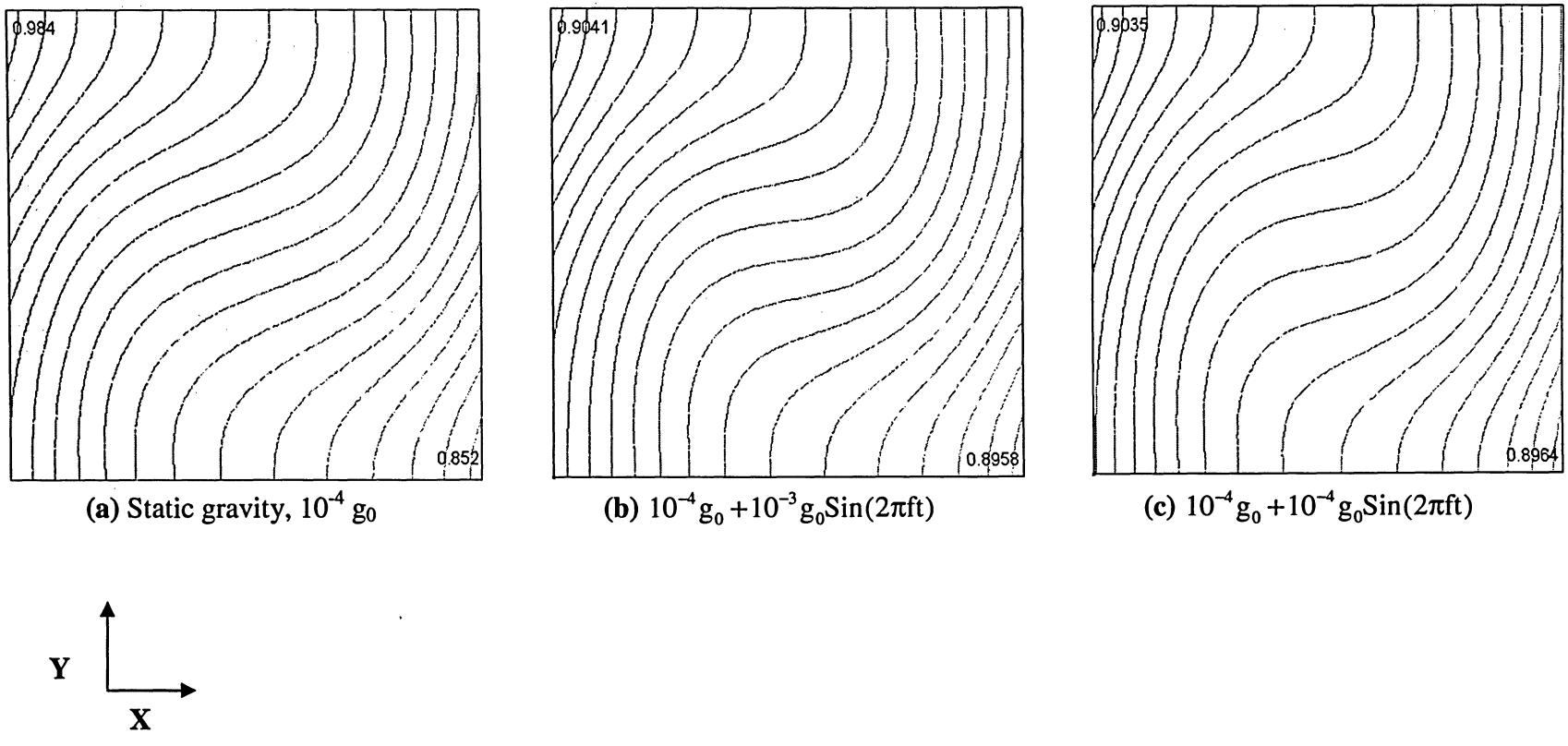

(a) Static gravity, $10^{-4}\ g_0$ **(b)** $10^{-4}g_0 + 10^{-3}g_0 Sin(2\pi ft)$ **(c)** $10^{-4}g_0 + 10^{-4}g_0 Sin(2\pi ft)$

Figure 4.8: Comparison of concentration contours (ΔC) for different g-jitters.

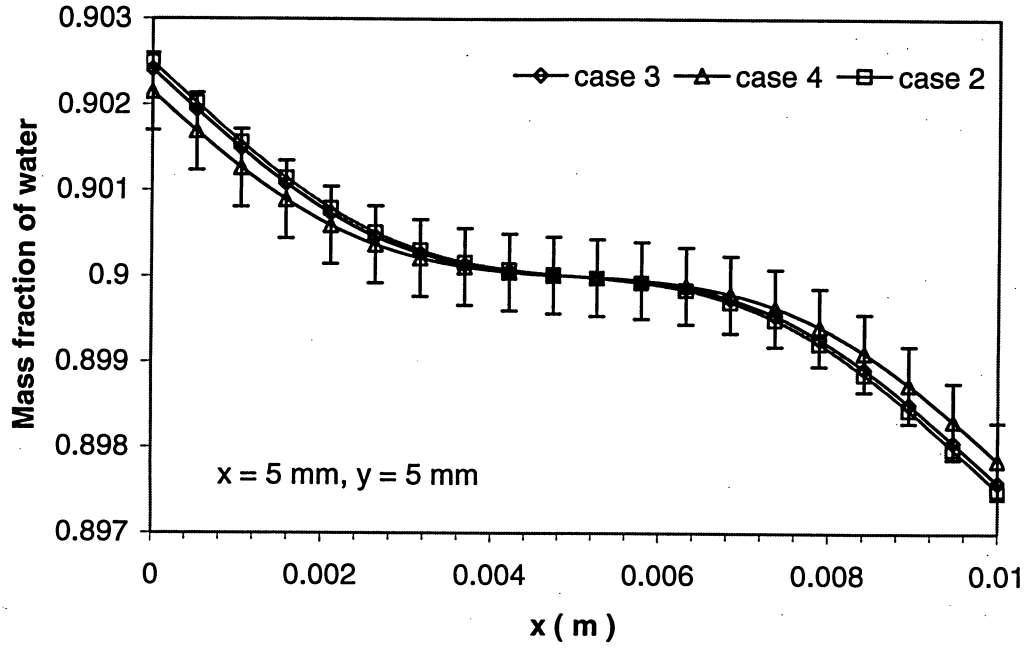

Figure 4.9: Comparison of water concentration along the X axis for different cases.

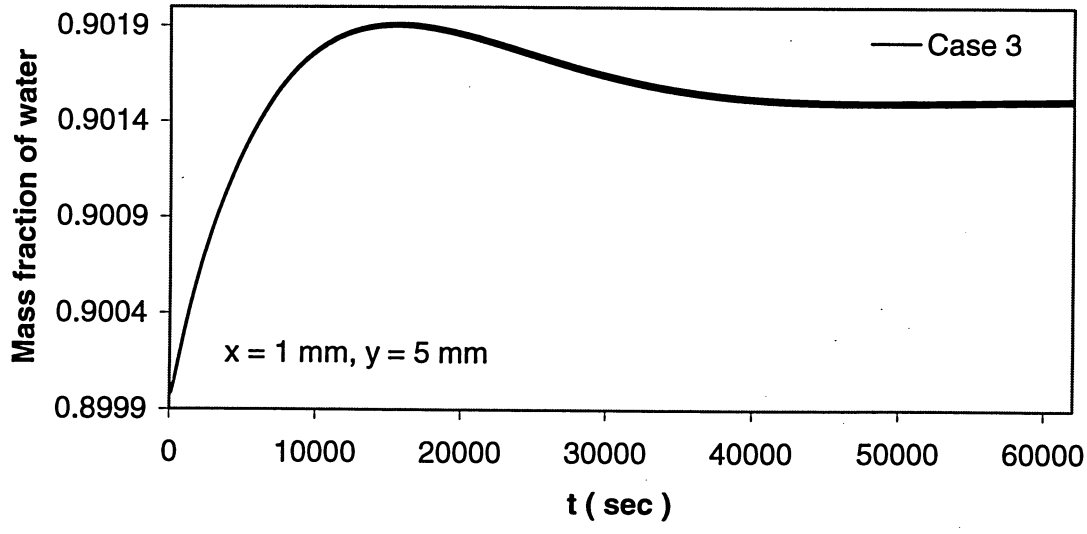

Figure 4.10: Time variation of water concentration for case 3.

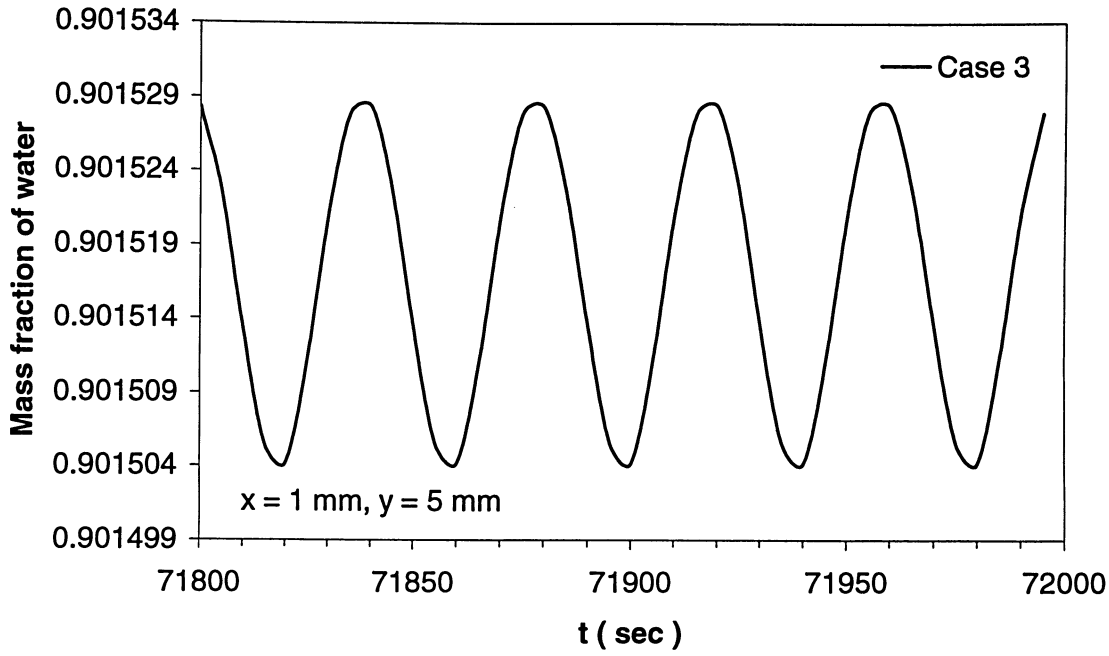

Figure 4.11: Time variation of water concentration for case 3 (last few time steps).

4.4 Summary

This chapter investigates the effects of low frequency vibrations on the thermal diffusion in a binary mixture. The binary mixture is made of water – isopropanol at 90: 10 wt %. In the analysis four cases with different levels of residual and oscillatory gravities have been modeled. The different cases analyzed are g-jitters with only pure oscillatory components, with only static gravity, and a combination of both. The static residual gravity causes a very strong fluid flow which depends on the magnitude of the residual gravity. This induces strong convection which remixes the fluid mixture resulting in an imperfect developed Soret separation. This is more pronounced at large static residual gravities. Therefore, the accuracy of the diffusion measurement gets affected greatly under such conditions. In the cases where oscillatory g-jitters are present the flow field is characterized by the oscillating convection. When the static residual gravity exists simultaneously with the oscillatory g-jitter component the flow field gets enhanced. The

effect of convection on the concentration distribution becomes very dramatic which in turn affects the fluctuation of the Soret separation. Similarly, the convection also affects the temperature field, which shows a larger deviation from the ideal linear distribution. Therefore, it may be concluded that g-jitters have a much harmful effect on the thermal diffusion process.

CHAPTER 5

EFFECTS OF STATIC GRAVITY ON THE THERMAL DIFFUSION PROCESS IN TERNARY MIXTURES

This chapter investigates the effects of different gravity conditions on the thermal diffusion process in a ternary mixture which consist of methane, n-butane and dodecane at equimolar concentrations. The different gravity levels applied are:
(i) $g = 0$, (ii) $g = 10^{-2}\, g_0$ and (iii) $g = 10^{-6}\, g_0$.

5.1 Mathematical Model

The square cavity is filled with the ternary mixture of methane (1) – n-butane (2) – dodecane (3) each at a mass fraction of 33.3 %. The physical geometry of the square cavity is the same as discussed in Section 3.2. The two lateral walls are maintained at constant but different temperatures so that the temperature difference is 10 degrees. The horizontal walls are assumed to be adiabatic. The continuity, momentum and energy balance equations are the same as discussed in Section 3.3, except the mass balance equation, since a ternary mixture is studied in this case. The mass conservation equation for each of the components in terms of mass fraction C_1 (methane), C_2 (n-butane) is given by:

$$\frac{\partial C_i}{\partial t} + u\frac{\partial C_i}{\partial x} + v\frac{\partial C_i}{\partial y} = \left(D_{c_{ij}} \frac{\partial^2 C_i}{\partial x^2} + D_{T_j} \frac{\partial^2 T}{\partial x^2} \right) + \left(D_{c_{ij}} \frac{\partial^2 C_i}{\partial y^2} + D_{T_j} \frac{\partial^2 T}{\partial y^2} \right) \qquad (5.1)$$

where i = 1,2 and j = 1,2

Initial and boundary conditions are the same as discussed in Section 3.4. The full transient Navier-Stocks equations, coupled with energy and mass transfer equations were solved numerically using the Finite element method.

The physical properties of the ternary mixture are given in Table 5.1.

Table 5.1: Physical properties of methane-n-butane-dodecane mixture @ P = 35 MPa.

Parameters	Values	
Average density of the mixture (ρ_0) at 60°C	418.295 kg/m^3	
Initial composition	methane (1)	n-butane (2)
	0.333	0.333
Thermal expansion coefficient (β_T)	2.44 ×10^{-3} (1/K)	
Volumetric concentration expansion coefficient	β_{C1}	β_{C2}
	0.03	0.021
Molecular diffusion coefficient (m^2/s)	D_{11}	D_{12}
	0.1356 ×10^{-8}	0.270 ×10^{-8}
	D_{21}	D_{22}
	0.3688 ×10^{-8}	0.1064 ×10^{-8}
Thermal diffusion coefficient (m^2/s-K)	D_{T1}	D_{T2}
	0.1092 ×10^{-10}	0.2926 ×10^{-11}
Dynamic viscosity of the mixture (η) at 60°C	6.2731 ×10^{-5} Pa.s	
Specific heat (C_p)	2399 J/ (kg K)	
Thermal conductivity (k)	0.1054 W/ (m K)	

5.2 Results and Discussion

Three cases with different levels of static gravities have been modeled. They are: (i) g = 0, (ii) g = 10^{-2} g_0 and (iii) g = 10^{-6} g_0. Results are discussed below:

5.2.1 Effects of static gravity

Case 1 represents the situation where the cavity filled with the ternary mixture is subject to zero gravity level, g = 0. Figure 5.1 shows the variation of methane concentration horizontally along the middle of the cavity. It can be seen that the concentration of methane is high near the hot wall and goes on decreasing in a linear pattern towards the cold wall along the width of the cavity. Figure 5.2 shows the variation of n-butane concentration. The concentration increases linearly from the hot to the cold wall. Similar pattern can be seen in the case of temperature profile, see Figure 5.3. This linear variation shows that at zero gravity level, the Soret effect causes the separation in the mixture.

Case 2 represents the situation where the system under study is subject to 10^{-2} gravity level. Figure 5.4 and 5.5 display the horizontal variation of methane and n-butane concentrations, respectively, along the middle of the cavity. A major component separation takes place along the direction of the temperature gradient in the vicinity of the hot and cold walls; whereas a homogenous mass distribution is found in the centre of the cavity. It can be observed that a boundary layer is formed near the hot and cold walls. The thickness of the boundary layers was found to be about 1 mm. This may be explained by the fact that the residual gravity initiates a mixing in the cavity due to the effect of the buoyancy force. It causes a strong clockwise flow in the cavity with velocities in the order of 10^{-5} m/s; see Figure 5.6. As the magnitude of the static gravity is increased, such mixing becomes very dramatic and the boundary layer structure becomes more prominent.

Figure 5.7 displays the temperature profile in the cavity at 10^{-2} gravity level. The temperature profile is completely distorted in this case. A sharp increase and a sharp decrease in temperature can be observed near the hot and the cold walls respectively whereas the temperature remains equal to its mean value in the central and very large portion of the cavity. The significant horizontal temperature gradient observed near the vertical walls can be explained due to the strong buoyancy convection.

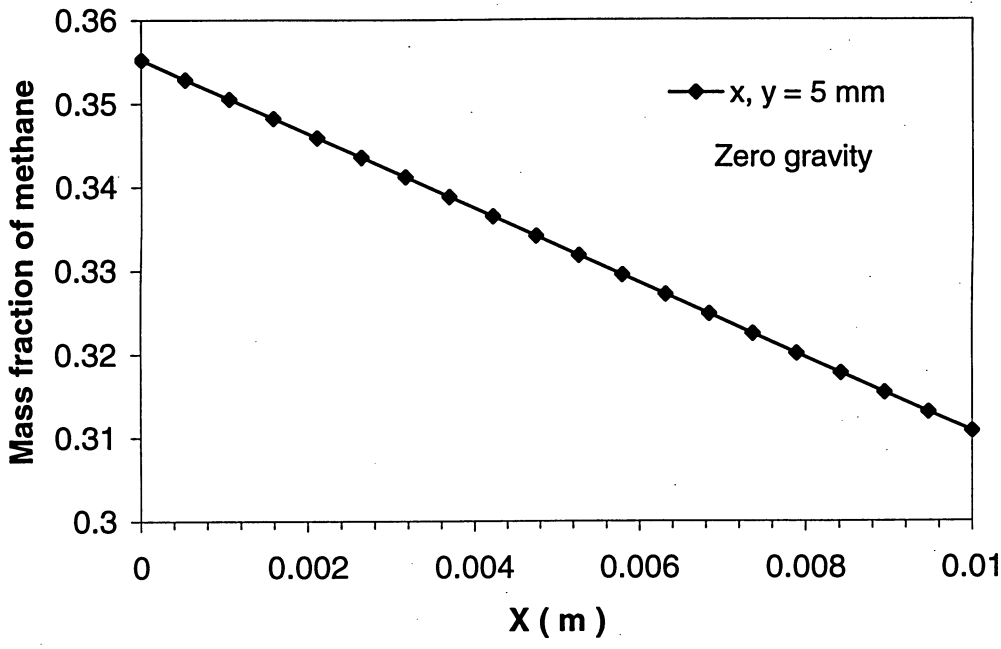

Figure 5.1: Concentration variation of methane at zero gravity level.

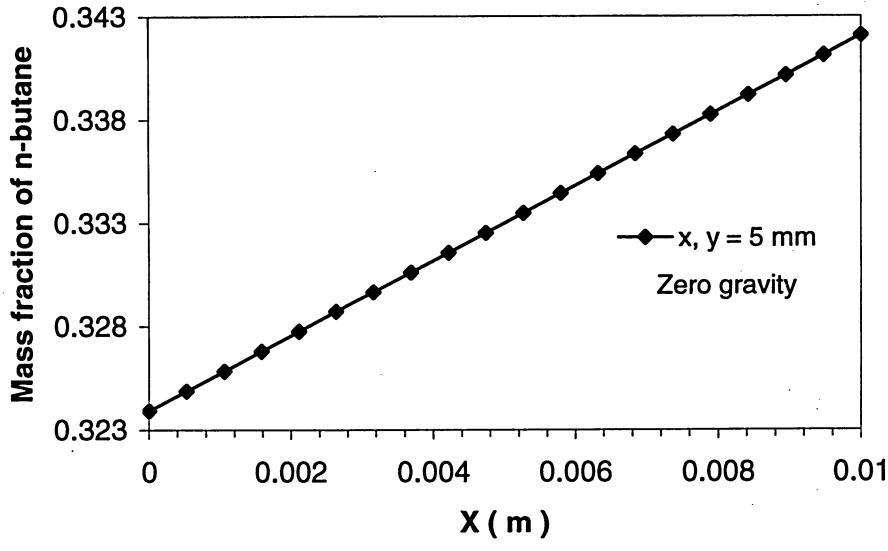

Figure 5.2: Concentration variation of n-butane at zero gravity level.

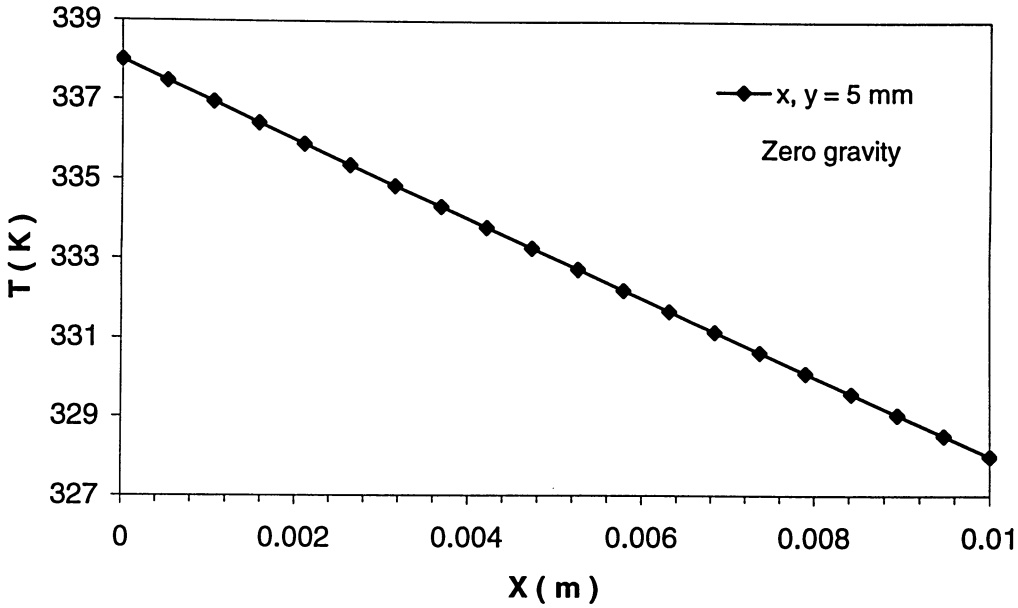

Figure 5.3: Temperature distribution along the cavity at zero gravity level.

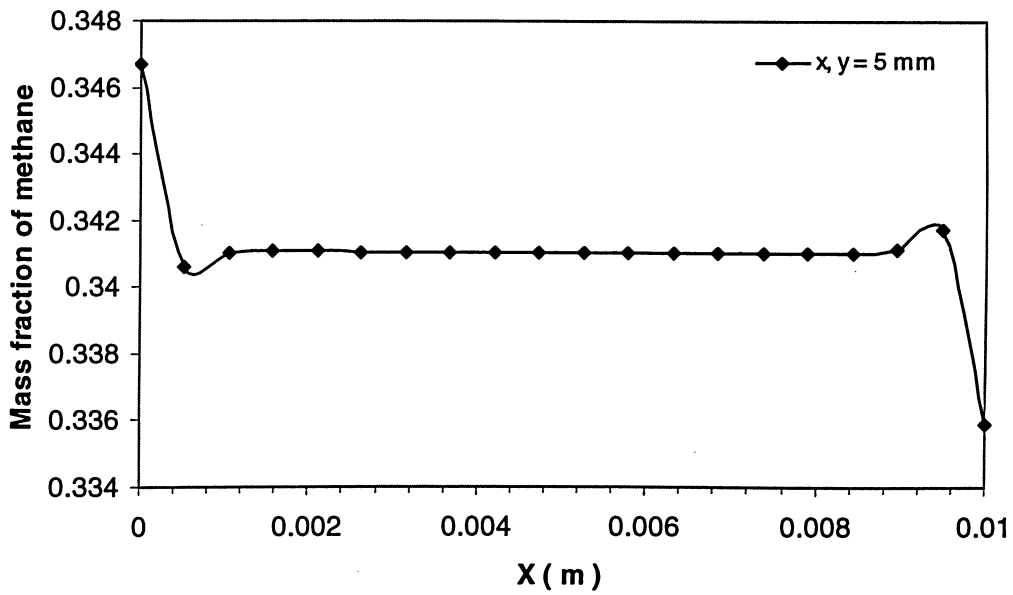

Figure 5.4: Concentration variation of methane at $g = 10^{-2} g_0$.

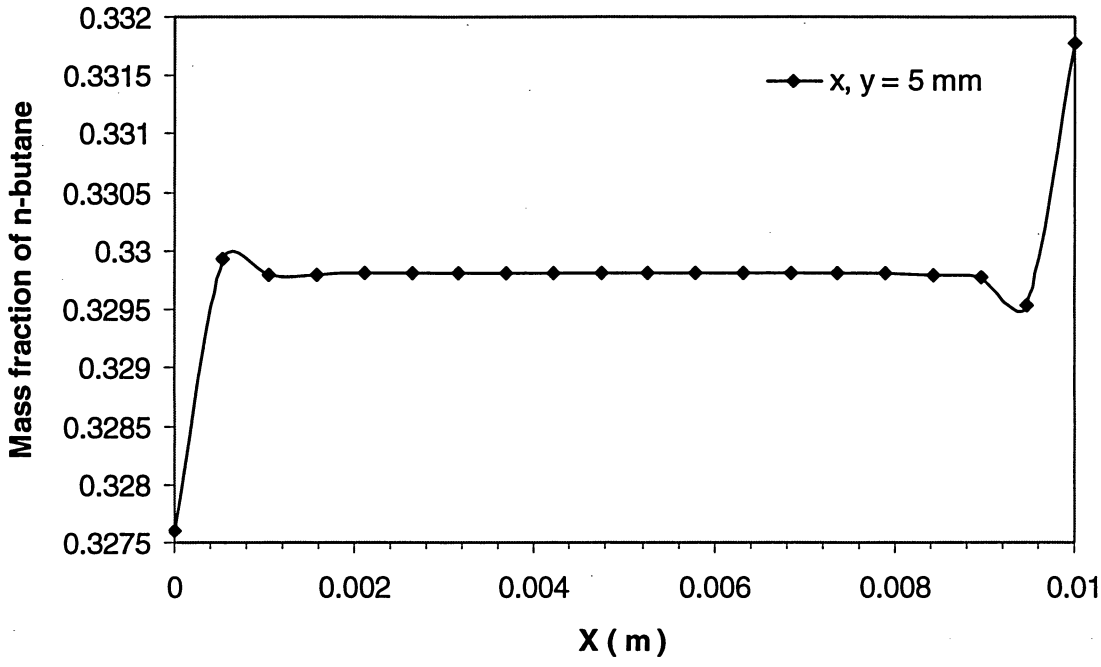

Figure 5.5: Concentration variation of n-butane at $g = 10^{-2} g_0$.

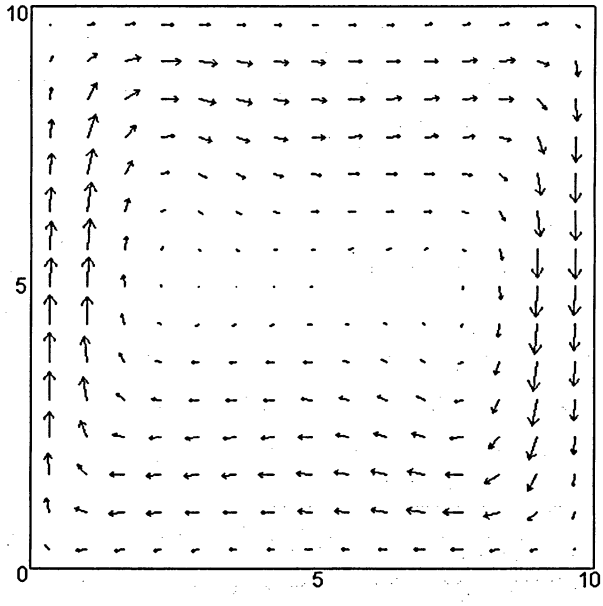

Figure 5.6: Velocity vector within the cavity.

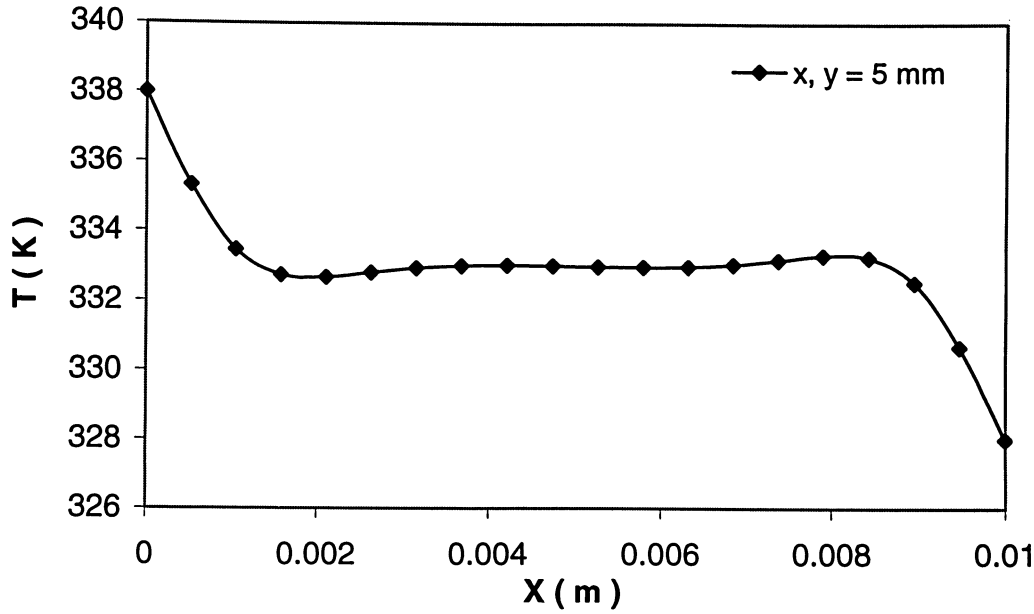

Figure 5.7: Temperature distribution along the cavity at $g = 10^{-2}\ g_0$.

Case 3 represents the situation when the system is subjected to micro gravity, $10^{-6}\ g_0$. Figure 5.8 and 5.9 displays the mass fraction variation of methane and n-butane, respectively, at $g = 10^{-6}\ g_0$ condition. Methane concentration gradually decreases from the hot wall towards the cold wall, whereas n-butane concentration increases along the width towards the cold wall. The concentration variation follows an almost linear pattern. Figure 5.10 depicts the temperature profile and it can be noted that the temperature profile also follows the same patter; almost linear. This can be explained by the fact that as the magnitude of gravity approaches zero gravity level the concentration as well as temperature profile tends to follow the zero gravity patterns.

Figure 5.11 compares the concentration variation of methane within the cavity for different gravity levels. For the $10^{-2}\ g_0$ case, a boundary layer is developed near the hot and cold walls. Methane tends to move towards the hot wall. At zero gravity level, concentration as well as temperature varies linearly. At microgravity level, $10^{-6}\ g_0$, the phenomenon tends to follows the zero gravity patterns. This can be explained by low magnitude of applied gravity level, i.e. it approaches the zero gravity level. It can be noticed that n-butane followed similar patterns.

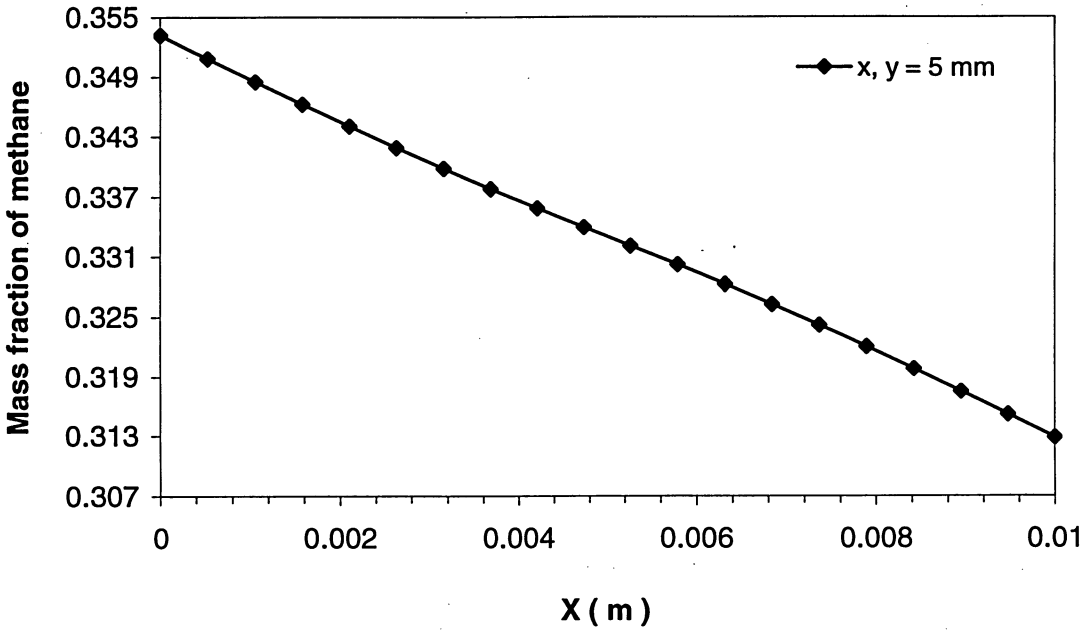

Figure 5.8: Concentration variation of methane at g = 10^{-6} g_0.

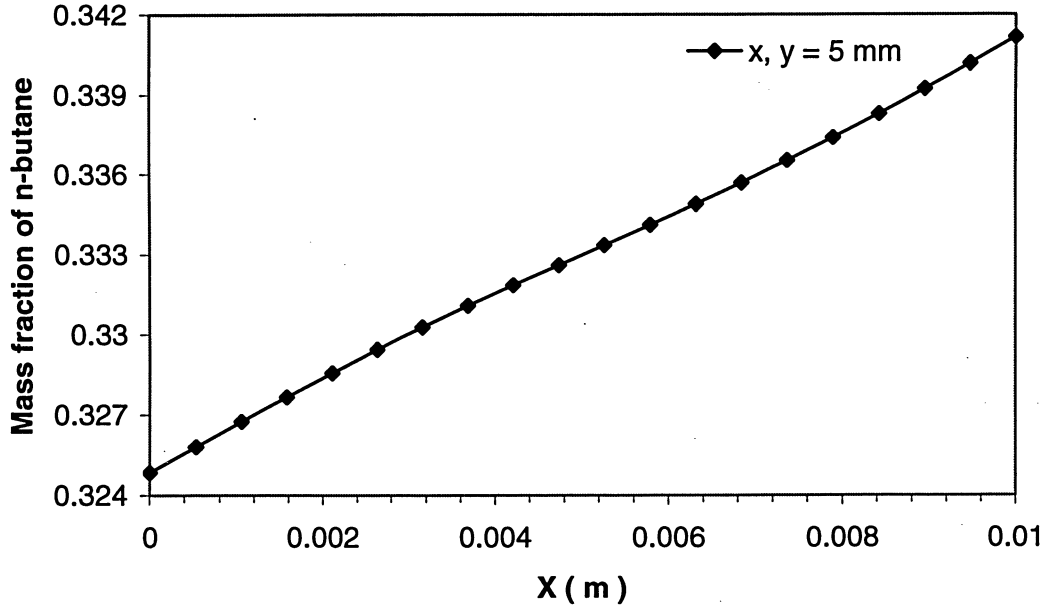

Figure 5.9: Concentration variation of n-butane at g = 10^{-6} g_0.

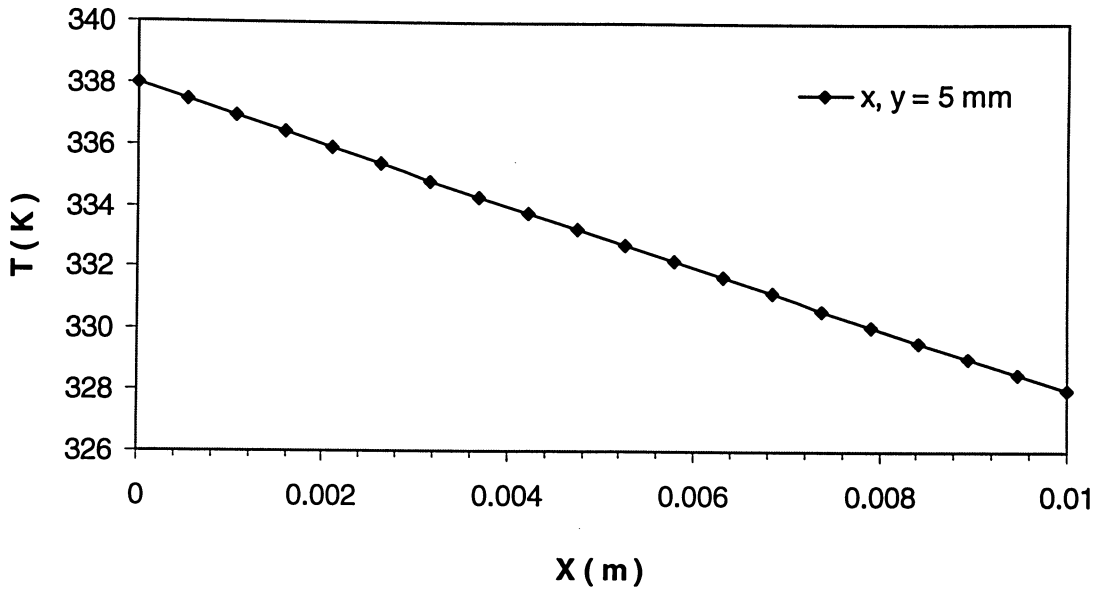

Figure 5.10: Temperature distribution along the cavity at $g = 10^{-6} g_0$.

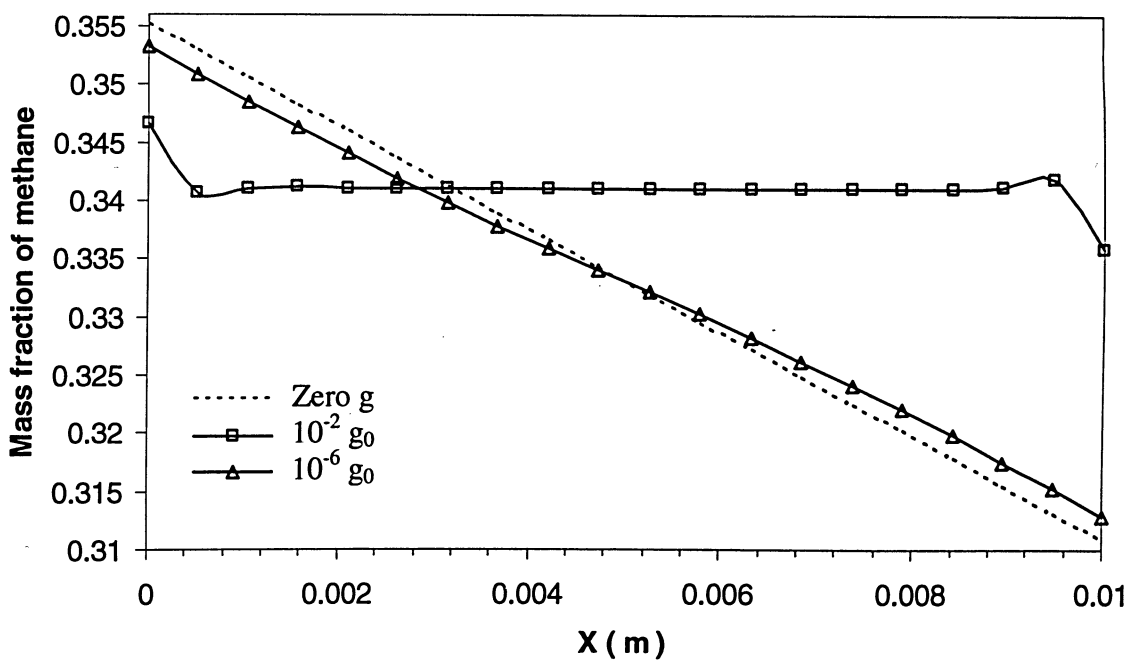

Figure 5.11: Comparison of concentration profiles under different levels of gravities.

5.3 Summary

In this chapter the effects static gravity on the thermal diffusion process in a single phase ternary mixtures was studied. The ternary mixture consists of methane -n-butane - dodecane (equal mass fractions). In the analysis, component concentration profiles, temperature profiles and velocity in the cavity were used to investigate the effect of static gravity on the thermal diffusion phenomena. From the results obtained, it can be inferred that as the gravity level decreases, the buoyancy convection is reduced and the maximum component separation could be attained in the absence of gravity. Furthermore, it can be concluded that the effects of the static gravity on thermal diffusion is very significant and buoyancy convection affects the Soret separation.

CHAPTER 6

CONCLUSIONS AND RECOMMENDATIONS

In this thesis, the effects of static and oscillatory gravities on the thermal diffusion process in different mixtures have been studied in detail. A two dimensional square cavity has been considered with lateral heating conditions. The full transient Navier-Stokes equations, coupled with energy and mass transfer equations were solved numerically by the Finite Element Method using the commercial software COMSOL. Several cases have been examined and they include: (i) two binary mixtures subject to different static gravities, (ii) a binary mixture subject to oscillatory gravities and finally (iii) ternary mixture subject to different static gravities. The components that constitute the mixtures include: methane, n-butane and dodecane; and water and isopropanol. In the analysis, component concentration profiles, temperature profiles and velocity in the cavity were used to investigate the effect of different gravity levels on the thermal diffusion phenomena.

In the first case, two binary mixtures were under study which consists of methane – n-butane (20:80 wt %) and water – isopropanol (90:10 wt %). For the 10^{-2} g_0 case, it was found that a boundary layer was developed near the hot and cold walls. Methane moved towards the hot wall; whereas n-butane towards the cold wall. At 10^{-3} g_0 level the boundary layers near the walls smoothen and tend to follow the linear pattern. At microgravity level, 10^{-6} g_0, it is found that the phenomenon tends to follow the zero gravity patterns. The analysis reveals a consistent behaviour between the two binary mixtures. From the analysis it can be inferred that the residual gravity will initiate a mixing in the cavity due to the effect of the buoyancy force. It can be concluded that the effects of the static gravity on thermal diffusion were very significant and buoyancy convection have a significant effect on the species separation. Also, upon comparison with the data reported by Chacha *et al.*, the results from this study were found to be in good agreement.

In the second case, the effects of static and oscillatory gravities on the thermal diffusion process in water – alcohol mixture (90:10 wt %) was investigated. Once again, a two-dimensional numerical model was used in the numerical simulation. The different cases analyzed were g-jitters with only pure oscillatory components, with only static gravity, and a combination of both. The static residual gravity caused a very strong fluid flow depending on the magnitude of the residual gravity. This fluid flow induced a strong convection which caused the remixing of the fluid mixture resulting in an imperfectly developed Soret separation. This effect was found to be more prominent at large static residual gravities. In the cases where oscillatory g-jitters were present the flow field was characterized by the oscillating convection. When the static residual gravity exists simultaneously with the oscillatory g-jitter component the flow field got enhanced. The effect of convection on the concentration distribution became very dramatic which in turn affected the fluctuation of the Soret separation. Similarly, temperature field was also affected by the convection, which showed a larger deviation from the ideal linear distribution. Therefore, it may be concluded that g-jitters have a much harmful effect on the thermal diffusion process when compared to that of the oscillatory gravity with same magnitude. Hence it is very important to eliminate static (residual) gravities in microgravity experiments while studying the diffusion of fluid mixtures.

Finally the effects of static gravities on a ternary mixture which consisted of methane – n-butane – dodecane at equal concentrations were investigated. The lighter component, methane, moves towards the hot wall and n-butane towards the cold wall while dodecane tends to remain in the middle of the cavity. The ternary mixture's behaviour is similar to the binary mixture for the zero and 10^{-2} gravity levels. However, at 10^{-6} gravity level, the concentration and temperature profile varies slightly from that of the binary mixture case. This could be attributed to the presence of one more component, dodecane, which would change the transport properties. The analysis also reveals that when the gravity level is decreased, the buoyancy convection is reduced and maximum component separation can be obtained. And also the computational time for the numerical solution was reduced dramatically.

For further study, it would be interesting to analyze the thermal diffusion process for different mixtures of various concentrations in a three dimensional cavity – which would be more realistic. And also, the physical properties like density, and transport coefficients could be considered as variables.

REFERENCES

[1] Chacha, M., Saghir, M.Z, Van Vaerenbergh, S, Legros, J.C, (2003). Influence of thermal boundary conditions on the double diffusive process in a binary mixture, Philosophical Magazine, 83:17–18, 2109 – 2129

[2] Trevoy, D.J., Drickamer, H.G., (1949). Thermal diffusion in binary liquid hydrocarbon mixtures, Journal of chemical physics, 17:11, 1120 – 1124

[3] Lorenz, M. and Emery, Jr. A. H., (1959). The Packed Thermal Diffusion Column, Chemical Engineering Science, 11:1, 16 - 23

[4] Kohler, W. and Muller, B., (1995). Soret and Mass Diffusion Coefficients of Toluene/n-Hexane Mixtures, J. Chem. Phys., 103:10, 4367 - 4370

[5] Leppla, C., and Wiegand, S., (2003). Investigation of the Soret effect in binary liquid mixtures by thermal-diffusion-forced Rayleigh scattering, Philosophical Magazine, 83:17–18

[6] Kohler, W. and Wiegand, S., (2002). Thermal Nonequilibrium Phenomena in Fluid Mixtures, Springer, Berlin

[7] Perronacea, A., Leppla, C., Leroy, F., Rousseau, B., Wiegand, S., (2002). Soret and mass diffusion measurements and molecular dynamics simulations of n-pentane– n-decane mixtures, Journal of Chemical Physics, 116:9, 3718 – 3729

[8] Zhang, K. J., Briggs, M. E., Gammon, R. W., and Sengers, J. V., (1996). Optical measurement of the Soret coefficient and the diffusion coefficient of liquid mixtures, Journal of Chemical Physics, 104:17, 6881 - 6892

[9] Jamet, Ph., Fargue, D., Costeseque, P., (1996). Determination of the Effective Transport Coefficients for the Separation of Binary Mixtures of Organic Compounds into Packed Thermal Diffusion Columns, Chemical Engineering Science, 51: 19, 4463 - 4475

[10] Costeseque, P., Gaillard, S., Gachet, Y., Jamet, Ph., (2003). Determination of the apparent negative Soret coefficient of water-10% alcohol solutions by experimental and numerical methods in packed cells, Philosophical Magazine, 83:17–18, 2039 – 2044

[11] Platten, J.K., Bou-Ali, M. M., Costeseque, P., Dutrieux, J. F., Kohler, W., Leppla, C., Wiegand, S., Wittko, G., (2003). Benchmark Values for Soret, Thermal Diffusion and Diffusion Coefficients of Three Binary Organic Liquid Mixtures, Philosophical Magazine, 83, 1965 – 1971

[12] Costeseque, P., Loubet, J.C., (2003). Measuring the Soret coefficient of binary hydrocarbon mixtures in packed thermogravitational columns (contribution of Toulouse University to the benchmark test), Philosophical Magazine, 83:17–18, 2017 – 2022

[13] Dutrieux, J.F., Platten, J.K., Chavepeyer, G., Bou-Ali, M.M., (2002). On the measurement of positive Soret coefficients, Journal of Physical Chemistry B, 106, 6104 – 6114

[14] Shukla, K., Firoozabadi A., (1998). A new model of thermal diffusion coefficients in binary hydrocarbon mixtures, Industrial & Engineering Chemistry Research, 37:8, 3331 – 3342

[15] Simon, J.M., Dysthe, D.K., Fuchs, A.H., Rousseauhave, B., (1998). Thermal diffusion in alkane binary mixtures - A molecular dynamics approach, Fluid Phase Equilibria, 150–151, 151–159

[16] Leahy-Dios, A., Bou-Ali, M.M., Platten, J.K., Firoozabadi, A., (2005). Measurements of molecular and thermal diffusion coefficiens in ternary mixtures, Journal of chemical physics, 122, 234502: 1 – 12

[17] Kita, R., Wiegand, S., Luettmer-Strathmann, J., (2004). Sign change of the Soret coefficient of polyethylene oxide in water-ethanol mixtures observed by thermal diffusion forced Rayleigh scattering, Journal of Chemical Physics, 121:8, 3874 – 3885

[18] Kempers, L.J.T.M., (2001). A comprehensive thermodynamic theory of the Soret effect in a multi component gas, liquid or solid, Journal of chemical physics, 115:14, 6330 – 6341

[19] Haughen, K.B., Firoozabadi, A., (2005).On measurement of thermal diffusion coefficients in multicomponent mixtures, The Journal of Chemical Physics, 122, 014516:1 – 7

[20] Gershuni, G.Z., Zhukhovitsky, E.M., (1981). Convective Instability of a Fluid in a Vibration Field under Conditions of Weightless, Fluid Dynamics, 16:4, 498-504

[21] Savino, R., (2002). Residual-g and g-jitter effects on the measurement of thermophysical properties in microgravity, Advanced Space Research, 29:4, 559 - 568.

[22] Chacha, M., Faruque, D., Saghir, M.Z., Legros, J.C., (2002). Solutal thermodiffusion in binary mixture in the presence of g-jitter, International Journal of Thermal Sciences, 41:9, 899 – 911

[23] Savino, R., Monti, R., (1999). Convection induced by residual-g and g-jitters in diffusion experiments, International Journal of Heat and Mass Transfer, 42, 111 - 126

[24] Monti, R., Savino, R., Alterio, G., (1997). Modelling and simulation of g-jitter effects on fluid science experimentation - Impact on the utilization of the ISS, Acta Astronautica, 40:2-S, 369 - 381

[25] Monti, R., Savino, Lappa, M., (2001). On the convective disturbances induced by g-glitter on the space station, Acta Astronautica, 48:5-12, 603-615

[26] Haase R., (1969). Thermodynamics of Irreversible Processes, Chapter 4, Addison Wesley, London

[27] Rutherford, W.M. and Roof, J.G., (1959). Thermal Diffusion in Methane n-Butane Mixture in the Critical Region, J. Phys. Chem., 63, 1506-1511

[28] Dougherty, E. L., Drickamer, H. G., (1955). Thermal Diffusion and Molecular Motion in Liquids, Journal of Physical Chemistry, 59, 443-449

[29] Kempers L.J.T.M., (1989). A Thermodynamic Theory of the Soret Effect in a Multicomponent Liquid, J. Chem. Phys., 90:11, 6541-6548

[30] Versteeg, H.K, (1995). An introduction to computational fluid dynamics, the finite volume method, Prentice Hall

[31] Chung, T.J., (2002). Computational Fluid dynamics, Cambridge University Press

[32] Saghir, M.Z., Yan, Y., Pan, S., (2005). Influence of vibrations on diffusion in liquids, a report to the Canadian Space Agency, Rep # 9F007-026020/001/SR

APPENDIX

The full transient Navier-Stokes equations, coupled with energy and mass transfer equations along with the boundary conditions were solved numerically using the Finite Element software FEMLAB. The codes used are given here.

Methane – n-butane mixture, $g = 10^{-6} g_0$

```
% Generated by FEMLAB 3.1i (FEMLAB 3.1.0.163, $Date: 2005/04/07 13:19:21
$)

flclear fem

% Femlab version
clear vrsn
vrsn.name = 'FEMLAB 3.1';
vrsn.ext = 'i';
vrsn.major = 0;
vrsn.build = 163;
vrsn.rcs = '$Name:  $';
vrsn.date = '$Date: 2005/04/07 13:19:21 $';
fem.version = vrsn;

% Geometry
g1=square2('.01','base','corner','pos',{'0','0'},'rot','0');
clear s
s.objs={g1};
s.name={'SQ1'};
s.tags={'g1'};

fem.draw=struct('s',s);
fem.geom=geomcsg(fem);

% Initialize mesh
fem.mesh=meshinit(fem);

% Constants
fem.const={'Dc','0.433e-8','Dt','-0.455e-11'};

% Constants
fem.const={'Dc','0.433e-8','Dt','-0.455e-11'};

% Application mode 1
clear appl
appl.mode.class = 'FlPDEG';
appl.dim = {'c','c_t'};
appl.assignsuffix = '_g';
clear bnd
bnd.type = 'neu';
bnd.ind = [1,1,1,1];
appl.bnd = bnd;
clear equ
equ.init = {{0.2;0}};
equ.f = '-u*cx-v*cy';
equ.ga = {{{'-Dc*cx-Dt*Tx';'-Dc*cy-Dt*Ty'}}};
```

```
equ.ind = [1];
appl.equ = equ;
fem.appl{1} = appl;

% Application mode 2
clear appl
appl.mode.class = 'ConvCond';
appl.module = 'ChEM';
appl.assignsuffix = '_cc';
clear prop
prop.weakconstr=struct('value',{'off'},'dim',{{'lm3'}});
appl.prop = prop;
clear bnd
bnd.T0 = {0,338,328};
bnd.type = {'q0','T','T'};
bnd.ind = [2,1,1,3];
appl.bnd = bnd;
clear equ
equ.init = 333;
equ.k = 0.095;
equ.rho = 452.092;
equ.C = 2040;
equ.u = 'u';
equ.v = 'v';
equ.sdiff = 'off';
equ.ind = [1];
appl.equ = equ;
fem.appl{2} = appl;

% Application mode 3
clear appl
appl.mode.class = 'NavierStokes';
appl.module = 'ChEM';
appl.gporder = {4,2};
appl.cporder = {2,1};
appl.assignsuffix = '_ns';
clear prop
prop.weakconstr=struct('value',{'off'},'dim',{{'lm4','lm5'}});
appl.prop = prop;
clear pnt
pnt.p0 = {0,35e6};
pnt.pnton = {0,1};
pnt.ind = [2,1,1,1];
appl.pnt = pnt;
clear equ
equ.gporder = {{1;1;2}};
equ.cporder = {{1;1;2}};
equ.init = {{0;0;35e6}};
equ.rho = 452.092;
equ.eta = 7e-5;
equ.F_y = '-452.092*9.81e-2*(1-(2.0849e-3*(T-333))+(0.714899*(c-0.2)))';
equ.ind = [1];
appl.equ = equ;
fem.appl{3} = appl;
fem.border = 1;

% Multiphysics
fem=multiphysics(fem);

% Extend mesh
fem.xmesh=meshextend(fem);

% Solve problem
fem.sol=femtime(fem, ...
```

```
                'solcomp',{'c','u','T','p','v'}, ...
                'outcomp',{'c','u','T','p','v'}, ...
                'tlist',[0:300:12600], ...
                'tout','tlist');

% Save current fem structure for restart purposes
fem0=fem;
```

Code used for water – isopropanol, $g = 10^{-3} g_0$

```
% Generated by FEMLAB 3.1i (FEMLAB 3.1.0.163, $Date: 2005/04/07
13:19:21 $)

flclear fem

% Femlab version
clear vrsn
vrsn.name = 'FEMLAB 3.1';
vrsn.ext = 'i';
vrsn.major = 0;
vrsn.build = 163;
vrsn.rcs = '$Name:  $';
vrsn.date = '$Date: 2005/04/07 13:19:21 $';
fem.version = vrsn;

% Geometry
g1=square2('0.01','base','corner','pos',{'0','0'},'rot','0');
clear s
s.objs={g1};
s.name={'SQ1'};
s.tags={'g1'};

fem.draw=struct('s',s);
fem.geom=geomcsg(fem);

% Initialize mesh
fem.mesh=meshinit(fem);

% (Default values are not included)

% Application mode 1
clear appl
appl.mode.class = 'NavierStokes';
appl.module = 'ChEM';
appl.gporder = {4,2};
appl.cporder = {2,1};
appl.assignsuffix = '_ns';
clear pnt
pnt.p0 = {0,1};
pnt.pnton = {0,1};
pnt.ind = [2,1,1,1];
appl.pnt = pnt;
clear equ
equ.gporder = {{1;1;2}};
```

```
equ.cporder = {{1;1;2}};
equ.init = {{0;0;1}};
equ.rho = 984;
equ.eta = 1.38e-3;
equ.F_y = '-984*9.81e-2*(1-(3.1e-4*(T-333)))';
equ.ind = [1];
appl.equ = equ;
fem.appl{1} = appl;

% Application mode 2
clear appl
appl.mode.class = 'ConvCond';
appl.module = 'ChEM';
appl.assignsuffix = '_cc';
clear prop
prop.weakconstr=struct('value',{'off'},'dim',{{'lm3'}});
appl.prop = prop;
clear bnd
bnd.T0 = {0,338,328};
bnd.type = {'q0','T','T'};
bnd.ind = [2,1,1,3];
appl.bnd = bnd;
clear equ
equ.init = 333;
equ.k = 0.522;
equ.rho = 984;
equ.C = 3990.5;
equ.u = 'u';
equ.v = 'v';
equ.sdiff = 'off';
equ.ind = [1];
appl.equ = equ;
fem.appl{2} = appl;
fem.border = 1;

% Multiphysics
fem=multiphysics(fem);

% Extend mesh
fem.xmesh=meshextend(fem);

% Solve problem
fem.sol=femtime(fem, ...
                'solcomp',{'u','T','p','v'}, ...
                'outcomp',{'u','T','p','v'}, ...
                'tlist',[0:10:100], ...
                'tout','tlist');

% Save current fem structure for restart purposes
fem0=fem;
```